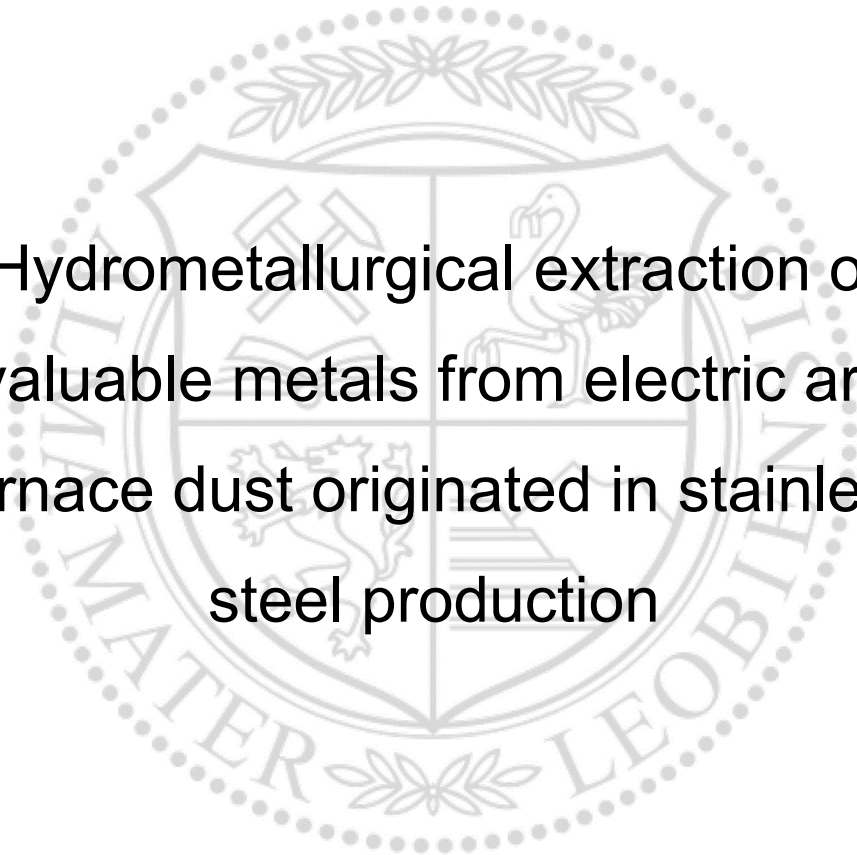Chair of Nonferrous Metallurgy

Master Thesis

Hydrometallurgical extraction of valuable metals from electric arc furnace dust originated in stainless steel production

Thomas Wolfgang Howard, BSc

Februar 2024

Acknowledgement

The first person I would like to thank, is my wife Alissa Shirley-Ann Howard, MSci for her support, never ending patience with me and all the love she gave and still gives me. Furthermore, I explicitly want to mention and thank at this point my loving and supporting parents Klaus and Elke Trost, as well as my dear brother Dipl.-Ing. Dr.mont. Claus O.W. Trost. Their support was crucial for my entire life, and I am grateful to have such a supportive family on which I can always rely on in times of need.

Moreover, I would like to thank my dear colleagues, whom I got to know during my studies at my alma mater in Leoben. Especially I want to mention Dipl.-Ing Manuel Schickbichler, Dipl.-Ing Julian Laschinger, Dipl.-Ing Patrick Krall, Dipl.-Ing Paola Vasold. Unfortunately, I am unable to mention all my friends here. Without all of them, my time in Leoben would have been way harder, less fun, and surely not as successful. I would not want to miss any of the countless hours of discussion, as well as the time we spend together having one or more beers.

I also would like to thank all my Professors, I had the pleasure to meet during my studies, for the knowledge I gained from their lectures and exams. Especially, I would like to mention and thank Priv.-Doz. Dipl.-Ing. Dr.mont. Stefan Steinlechner, Priv.-Doz. Dipl.-Ing. Dr.mont. Jürgen Antrekowitsch, Univ.-Prof. Dipl.-Ing. Dr.mont. Helmut Antrekowitsch as well as Priv.-Doz. Dr. Megan J. Cordill for their supervision and support. Tough some exams were hard during my studies they were always fair, and I gained a lot of knowledge while discussing the subject.

Without Dipl.-Ing. Gerald Haslinger, Dipl.-Ing. Christoph Wölfler, Dipl.-Ing. Christian Dornig and Dipl.-Ing. Kerrin Witt, my colleagues at the institute for Nonferrous Metallurgy, the time writing this thesis would have been harder. Furthermore, I would like to thank my fellow student worker Xenia Wimmer, without whom the experiments conducted in this thesis would have taken much longer. Moreover, I would like to thank Matthias Honner for his experience, which he gladly shared with me, and help with the application of ideas and for his involvement in planning of the whole experimental setup.

Furthermore, I would like to thank the federal Republic of Austria for a free education, which made it possible for me to get my university degree.

Finally, I would like to thank the federal state of Styria, which funded the project "HydroStäube" with the "Zukunftsfond Steiermark", which was the project for which this thesis was written for.

Abstract

Regarding the growing production rates of metals, there is also a direct proportional increase in the accumulation of corresponding by-products like dust. These often contain, as in the case of stainless steel production, valuable metal like Cr, Ni, and Mo, which would be lost if no actions would be taken. To counteract the resulting dependency on imports, material loss, economic and ecological effects, the interest in recycling of those residues has grown in the last decade. Though most industrially applied processes recover these metals from dust by pyrometallurgical means, the research in hydrometallurgical methods to recover metals has gained attention. This is due to the flexibility of such solutions in dealing with inhomogeneous input materials and the ease with which they can be adapted in their design. Therefore, a new hydrometallurgical approach in the extraction of Cr and Ni by dissolving stainless steel dust in five different acids has been conducted in the course of this thesis. Through these leaching experiments, the knowledge of the need for harsher conditions, like higher temperature, longer leaching time and higher acidity has been gained. Simultaneously, an optimized setup for such conditions was developed, that counteracts the disadvantages which were noticed while conducting the experimental campaigns. Based on these results and optimizations, future campaigns with and without pre-treatment of dusts to recover valuable metals by leaching and following precipitation steps, are in development.

Kurzfassung

Mit der steigenden Produktionsrate von Metallen nimmt auch die Anhäufung entsprechender Nebenprodukte wie Staub zu. Diese enthalten oft, wie im Fall der Edelstahlproduktion, wertvolle Metalle wie Cr, Ni und Mo, die verloren gehen könnten, wenn keine Maßnahmen ergriffen würden. Um der daraus resultierenden Abhängigkeit von Importen, finanziellen und materiellen Verlusten entgegenzuwirken, hat das Recycling dieser Rückstände im letzten Jahrzehnt an Interesse gewonnen. Obwohl die meisten industriell angewandten Verfahren diese Metalle auf pyrometallurgischem Wege aus dem Staub zurückgewinnen, hat die Erforschung hydrometallurgischer Methoden zur Rückgewinnung von Metallen an Aufmerksamkeit gewonnen. Dies ist auf die Flexibilität solcher Lösungen im Umgang mit inhomogenen Einsatzmaterialen und der leichten Adaption der Prozesse zurückzuführen. Daher wurde im Rahmen dieser Arbeit ein neuer hydrometallurgischer Ansatz für die Rückgewinnung von Cr und Ni durch Auflösen von Edelstahlstaub in fünf verschiedenen Säuren durchgeführt. Durch diese Laugungsversuche wurde das Wissen über die Notwendigkeit härterer Bedingungen, wie höhere Temperatur, längere Laugungszeit und höherer Säurekonzentration, gewonnen. Gleichzeitig erfolgte die Entwicklung eines optimierten Aufbaues für solche Bedingungen, der den Nachteilen entgegenwirkt, die bei der Durchführung der Versuchskampagnen festgestellt wurden. Basierend auf diesen Ergebnissen und Optimierungen sind zukünftige Kampagnen mit und ohne Vorbehandlung der Stäube zur Rückgewinnung von Wertmetallen durch Laugung und anschließende Fällungsschritte in der Entwicklung.

EIDESSTATTLICHE ERKLÄRUNG

Ich erkläre an Eides statt, dass ich diese Arbeit selbstständig verfasst, andere als die angegebenen Quellen und Hilfsmittel nicht benutzt, den Einsatz von generativen Methoden und Modellen der künstlichen Intelligenz vollständig und wahrheitsgetreu ausgewiesen habe, und mich auch sonst keiner unerlaubten Hilfsmittel bedient habe.

Ich erkläre, dass ich den Satzungsteil „Gute wissenschaftliche Praxis" der Montanuniversität Leoben gelesen, verstanden und befolgt habe.

Weiters erkläre ich, dass die elektronische und gedruckte Version der eingereichten wissenschaftlichen Abschlussarbeit formal und inhaltlich identisch sind.

Datum 12.02.2024

_____
Unterschrift Verfasser/in
Thomas Wolfgang Howard

Table of content

1 Introduction

"One man's trash is another man's treasure", is a quote which represents the daily struggle as well as the goal in the field of residual reprocessing and recycling research. In today's perspective of growing metal production and consumption, the amount of corresponding accruing by-products like dust, slag and sludge gradually increases with it. Environmental concerns of negative impact and interaction of such residues in landfills as well as surging interest in recovery of valuable metals, which would be lost otherwise, are of special interest. One such process with growing production rates and therefore arising amounts of residues is the **E**lectrical **A**rc **F**urnace (EAF). This steel making route uses steel scrap of different quality and quantity to produce a large portfolio ranging from low requirement construction to high-performance tool steel and stainless steel. From 2016 to 2021, where reliable data could be found, the average global growth rate of EAF produced crude steel was about 2.4 %/year [1]. This development can be traced back to the change in producing steel away from the carbon intensive route **B**last **F**urnace (BF) and **B**asic **O**xygen **F**urnace (BOF) to a less CO_2 emitting process like the EAF [2].

Via the EAF route, about 10-20 $kg_{dust}/t_{crude\ steel}$ is produced during the process of smelting and refining scrap to steel [3]. This can be applied to the 58.21 Mio t/year of stainless steel produced worldwide in 2021, which would result in 0.58 to 1.16 Mio t/year of stainless steel dust [4]. Through complex processes during smelting and metallurgical operations, dust is formed at different locations though various mechanisms at different rates [5–8]. These preconditions are the reason, why even for two similar melts, dust with different elemental composition and phase distribution is often analysed. The main elemental components of the dust are beside Fe and Zn as well as slag formers like Ca, Si, Mg, and Al all to a certain extent in their corresponding oxide form. In the case of special steels like tool and corrosion resistant steels, larger amounts of Cr, Ni, Mo as well as traces of W, Co, and V, can be found. Due to the complex nature of the forming of dust particles, the phases in which these elements are present can also vary in a larger spectrum. Usually, dust of lower steel quality, which is frequently coated to prevent corrosion, contains high amounts of Zn, and is recycled via the "Waelz kiln". This process focuses on Zn recovery through reduction, vaporization, and re-oxidation in the dedusting facility of the aggregate [9, 10]. In the case of stainless steel dust, this reactor and its metallurgical work is not a viable option. Most of the processes which are used to recover metals from these dusts are of pyrometallurgical nature, which are mostly carbon-based as well as at the same time energy intensive [11–13]. These apply different technological means to create the necessary conditions for the reduction, for instance plasma generators attached to a coke filled shaft furnace or self-reducing pellets in a rotary hearth

furnace [13–18]. In Europe, the "ScanDust" process from the company Befesa in Landskrona, Sweden is the most applied process. This means companies must store the potentially hazardous dust on company grounds and then ship it, in case of Austrian companies, through several states to Sweden with an adequate transporter for remelting it into a Fe-Cr-Ni alloy. Considering these mentioned aspects of the pyrometallurgical recycling routes, a hydrometallurgical recovery of valuable metals like Cr and Ni can offer cleaner, more flexible and energy efficient solutions. Therefore, the aim is to investigate a potential hydrometallurgical recycling process, precipitation steps for the recovery of the valuable metals as well as an analysis of potential of dust available for such a process Europe-wide. This thesis is a part of the mentioned research project, and the target is the development of a hydrometallurgical leaching step, in which valuable metals like Cr, Ni, Mo, V, and W can be dissolved. Therefore, eight different dusts from European stainless steelmaking companies were characterized and the most promising candidate was chosen for leaching. In these leaching experiments, five different acids were investigated as of their leaching potential and from the experience gained, an optimized experimental setup was developed.

2 Electric Arc Furnace

The following chapter will provide an overview over the electric arc furnace process in general and focus on the production of stainless steel. Moreover, a short overview of production statistics and average annual growing rates will be discussed. Furthermore, the formation and phases present in EAF dust will be explained in greater detail to understand how characterization must be performed.

2.1 Process description

The basic principle of the electric arc furnace process is smelting of pre-sorted steel scrap via the usage of electrical energy as well as providing enough energy for metallurgical operations. Hereby, steel scrap is fed via baskets into the refractory lined hearth, while the oven lid is shifted to the side and the graphite electrodes are in an elevated position. After the scrap is discharged, the lid shifts over the hearth again and the electrodes begin to move down towards the scrap. Before the electrodes make contact, arcs may form, electrically connecting the scrap and electrodes and begin to melt down the scrap. This first part of the energy transfer is not satisfactory for a fast melting. Therefore, for faster tap to tap times, smelting must be supported by natural gas burners, situated at the lower end of the lid. During this part of the process, slag formers like CaO, SiO_2, MgO, and Al_2O_3 are fed via hopper systems into the hearth. When a liquid slag forms at a later point during the melting period, the electrodes electrically conduct with the forming slag and resistance heating starts. This leads to lower energy losses, which can be lowered furthermore significantly with a foaming slag, which wraps the electrical arc and decreases thermal radiation losses. For such a foaming slag, the oxidation of [C] to {CO} is necessary. In the case of stainless steel, this negatively affect the metallurgical performance of Cr and other oxygen affine alloying elements and must be avoided. Therefore, metallurgical work, as well as decarburization, is performed after tapping in either an **A**rgon-**O**xygen-**D**ecarburization (AOD) converter or **V**acuum-**O**xygen-**D**ecarburization (VOD) ladle treatment. In these two processes, the [Cr] in the melt is protected against oxidation either through a low partial pressure of {CO} or vacuum. For this, the content of the EAF is tapped, and the raw stainless steel is poured into a transport ladle and transported to the mentioned process. Finally, the steel can undergo a refining and reheating step in a ladle furnace. After achieving the desired temperature for casting, the liquid steel is transported to either a continuous casting machine or to an ingot caster and solidifies for follow-up forming and machining. A schematic process flow chart for a stainless steel producing plant, a taken example from Böhler Edelstahl GmbH & KG, with aggregates for the production can be seen in Figure 1 [19]. To conclude, to produce this type of steel, companies usually apply an

ultra-high-power concept for the EAF, which means that this furnace main objective is melting the scrap and ferroalloys.
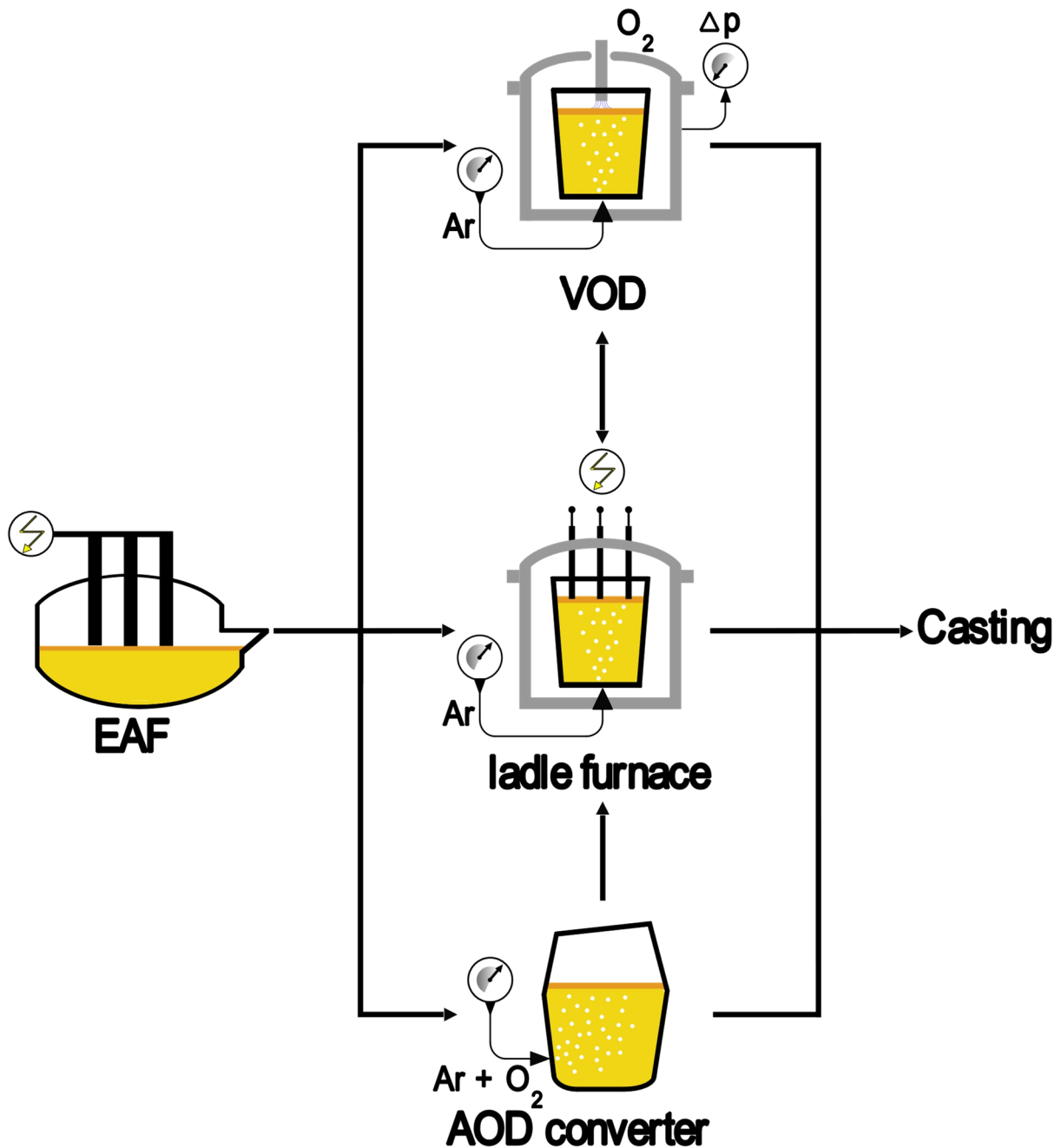

Figure 1: Schematic process flow of a stainless steel producing steel mill via EAF [19]

For achieving high contents of alloying elements in stainless steel production, two operational routs are commonly applied. The first uses only high-quality stainless steel scrap with an already satisfactory content of alloying elements, so that only fine-tuning with ferroalloys must be performed. By using high-quality stainless steel scrap, the costs for ferroalloys can be limited to a minimum. The other method uses low alloyed steel scrap as base material for producing stainless steel. To achieve the desired content of alloying elements during the smelting, ferroalloys are added in great quantity, so that the lower analysis limit can be

achieved. This way is only chosen, if low amounts of [P] as well as high [Cr] and [Mn] are a prerequisite for the steel. For this, ferroalloys are only added after [P] is oxidized, at the desired level and litigated in the slag, which itself must be ground off from the liquid steel and replaces by a non-oxidizing slag.

2.2 Stainless steel in general and production overview

Stainless steel or corrosion resistance steel is usually alloyed with a minimum of 10.5 % of Cr to form a thin Cr-Fe-oxide layer at the surface, which protects the steel from corroding. Depending on the content of C in the steel and its application, the content of Cr and other alloying elements like Ni, Mo, N and others may be at higher values, to ensure satisfactory corrosion properties. The recovery of these alloying elements from dust, sludge and slags are of special interest. The application of this steel grade is broadly positioned. They find usage in cutlery, surgical instruments, food processing, architecture, petrochemical, and energy appliances.
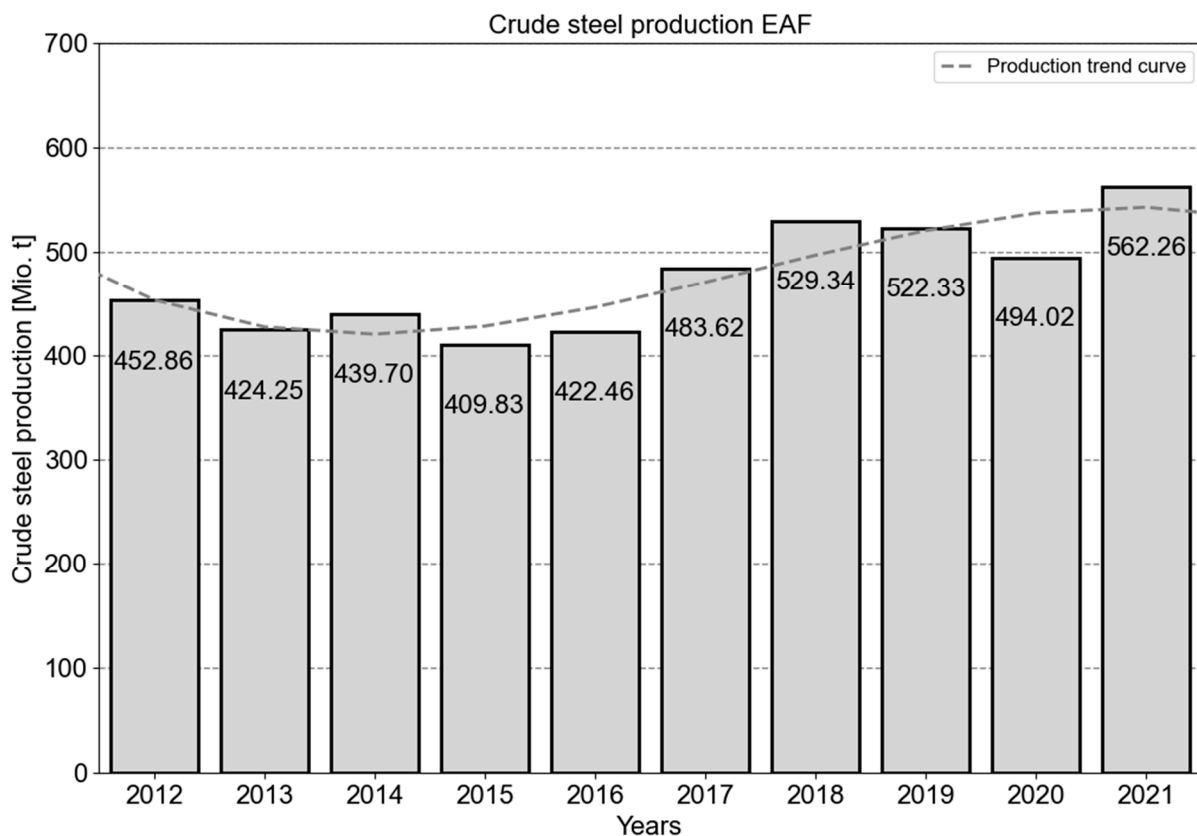

Figure 2: Annual world production of crude steel via the EAF route (2016-2021) [1]

As mentioned previously, the production of crude steel, including stainless steel, via the EAF is growing in the last years, as can be seen in Figure 2 and Figure 3. Observed can be a decline in production from 2012 to 2015, though some fluctuations are visible. A closer

expectation of Figure 2 reveals, that in the years 2016-2018 the growth was continuous until then, whereas 2019 shows a stagnant production output and 2020 even a dip in production. This dip could be traced back to pandemic related issues with production. For 2021, it appears that these issues have been not as influential and a growth in production can be observed. The resulting average annual growing rate for the crude steel production between 2012 and 2021 can be calculated as of 2.42 %/year [1].

When analysing the production data of stainless steel, a different pattern as described above can be observed in Figure 3. A nearly constant growth can be seen, represented by the trend line, which was calculated for the period of time data was available. Similarly, to crude steel, stainless steel production dipped in 2020 for the same reason and started growing again in 2021 as can be seen. The resulting average annual growing rate for stainless steel can be calculated as 6.23 %/year [4].
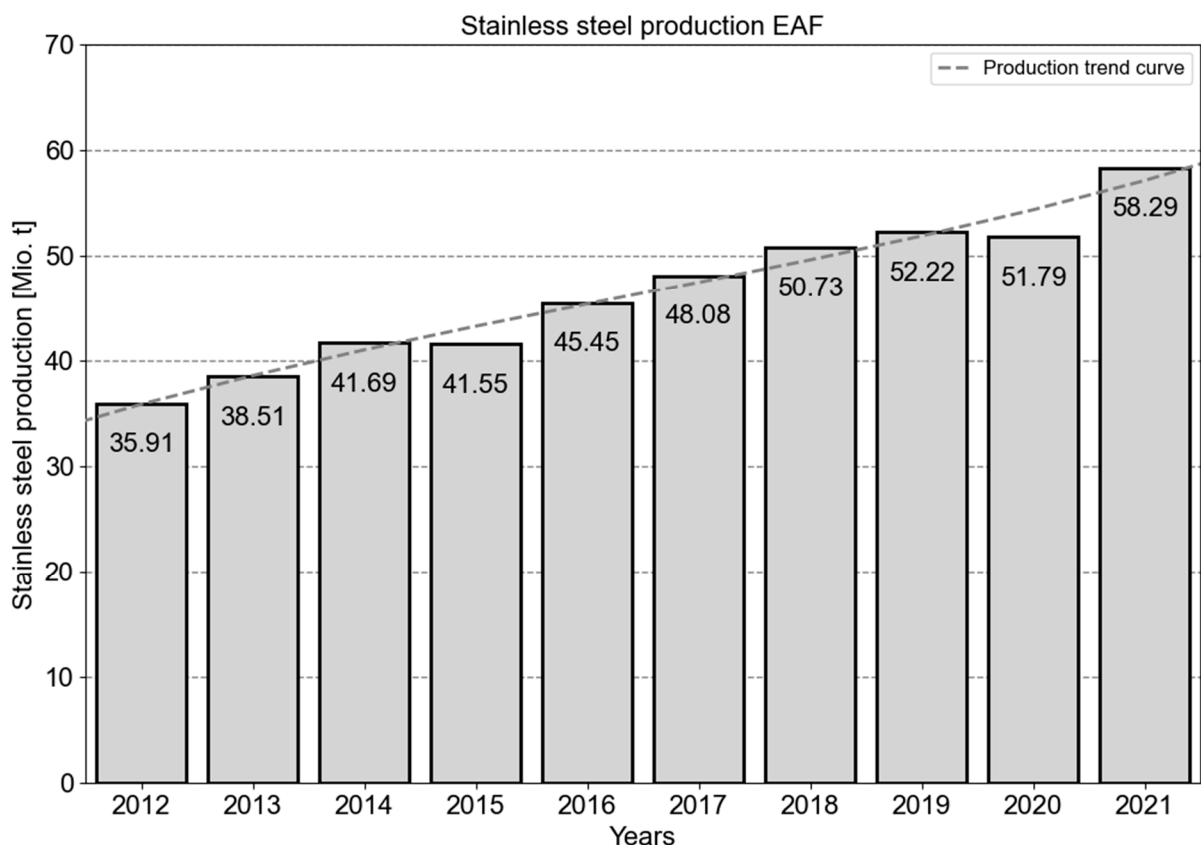

Figure 3: Annual world production of stainless steel via the EAF route (2016-2021) [4]

The latest available production data for World, European and Austrian production can be seen in Table 1 together with their average annual growing rates. The combination of the yearly production of stainless steel with the average range of 10-20 kg_{dust} per ton of steel in the EAF, results in a rough estimate of 0.58 and 1.16 Mio t/year of dust accumulation worldwide [3].

Table 1: Annual production of crude as well as stainless steel via EAF and their global growing rates between 2016 and 2021

	Production [Mio t/year]			Average growing rate [%/year]	Literature
	World	Europe	Austria		
Crude steel [1]	562 260	66 680	0.689	2.42 [2]	[1, 20]
Stainless steel	58.3	6.953	0.145[3]	6.23 [2]	[4, 20, 21]

[1] includes stainless steel, [2] calculated from production rate statistics of 2012-2021, [3] includes tool steel

2.3 EAF-Dust formation

Dust formation can occur at various stages of the process as well as at different locations in the EAF. Through one of the openings in the lid of the EAF, as portrayed in Figure 4, the freshly formed dust leaves the oven. In the flue gas pipe leading to the baghouse, the particles can attach themselves to the other particles and accumulate, which is indicated in the left upper corner of Figure 4.
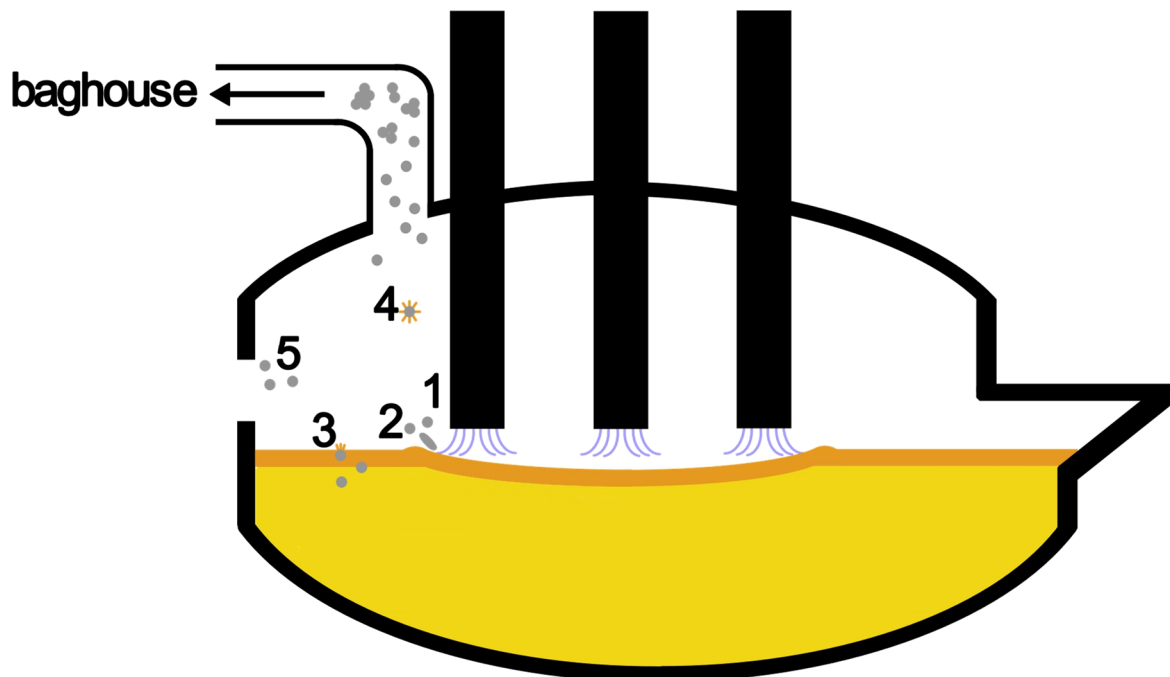

Figure 4: Formation mechanisms of dust in an EAF [5, 6]

At the beginning of the process, mainly fine particles from scrap and slag formers will contribute to the formation of dust. During the melting, the formation can be split into five different mechanisms, which contribute to varying degree. In Figure 4 these mechanisms are visualized and can be separated into the following zones:

- Zone 1: Volatilization of metals like Zn, Fe, Ni etc. especially around hot zones like arc or oxygen injection areas, which represent typical hotspots. Furthermore, this phenomenon can occur where bubbles rupture at the surface of the melt [5, 6].

7

- Zone 2: Emissions of droplets at the impact points of the arc from the steel bath [5, 6].
- Zone 3: Bursting of gas bubbles formed through reactions in the steel bath at the surface and resulting projection of fine droplets [5, 6].
- Zone 4: Bursting of gas bubbles carried into the oven room above the melt and oxidizing in the atmosphere [5, 6]. It is not definitely clear if this phenomenon occurs in the EAF.
- Zone 5: Directly carry over of solid particles when charged into the furnace (scrap, slag formers and coal) [5, 6].

The majority of the formed dust particles are often in sub mm to a few µm in diameter range as well as of spherical nature and some of them may be hollow [5, 8, 22]. On their way to the bag house agglomeration and further oxidation may occur, which leads to particle aggregation similar to Figure 10 (b) in a later chapter. Thus, they may occur in various shapes and sizes ranging from elongates grain like structure to spherical particles [22].

2.4 Present phases in EAF-Dust

As a result of the relative oxygen rich atmosphere, the majority of the identifiable phases are in the form of various oxides. These can range from single metal oxides to complex phases like spinel phases of various metals, as can be seen in Table 2. The formation of such spinel phases is likely to happen under the circumstances present in an EAF, which itself explains the predominance of such phases in those dusts [8, 22, 23].

Table 2: List of possible phases found in EAF-Dust according to literature

Chemical composition	Phase name	Literature
Fe_3O_4	Magnetite (Spinel)	[22, 24]
$FeCr_2O_4$	Chrome-Iron Spinel	[22, 24]
$NiFe_2O_4$	Nickel-Iron Spinel	[22, 24]
$ZnFe_2O_4$	Franklinite (Spinel)	[22, 25, 26]
ZnO	Zincite	[23, 25, 26]
$MnFe_2O_4$	Manganese ferrite (Spinel)	[22]
CaO	Calcia	[26]
SiO_2	Silica	[26]
MgO	Periclase	[26]
Al_2O_3	Alumina	[26]

Furthermore, some predominate phases like Fe_3O_4 might not be pure, like in their chemical form and a noticeable amount of the Fe atoms might be replaced with e.g. Cr, Ni and other metals [22]. This can also lead to difficulties when performing XRD-analysis, because of the tendency of these phases to broaden the peak of such mixed phases [22]. Moreover, this can

affect the identification of peaks, which might lead to misidentification or no identification of phase at all. The content of Zn rich phases in the dust may vary in lager margins depending on the type of steel produced and the scrap used for the remelting. Also, phases may exist in a variety in solid solution within each other and be harder to identify exactly [22].

3   State-of-the-art in EAF dust recycling

The recycling of EAF dust is manly focussed on the recovery of Zn, since only a fraction of the world production of steel is stainless [1, 20]. Usually processes like the "Waelz reactor" plays a vital role in the recycling of EAFD. The high Zn bearing EAFD are most commonly introduced into the Waelz process with the goal to reduce ZnO by carbothermic means, vaporize the Zn and re-oxidize it again in the gaseous phase [27]. This is performed in a rotary kiln in a counter current principle. A schematic drawing of the cross section of the process can be seen in Figure 5. In it, at the bottom of the kiln, a mixture of Fe-oxides, ZnO and carbon as reducing agent can be seen. Over the length of the rotary kiln, the C reacts with various oxides in the mixture and forms CO and CO_2 together with a metallic fraction. The resulting metallic Zn vaporizes, because of the temperatures present in the kiln, and gets carried over to the gaseous phase above the bed. This first gaseous Zone, as can be seen directly between the two dotted lines in the cross section of the kiln, consists of gaseous Zn and CO and prevents the oxidation of Zn directly above the bed. Above this Zone, the CO reacts to CO_2 with oxygen, which gets introduced at the lower end of the kiln via the gas burner. This oxidating atmosphere also re-oxidizes the gaseous Zn to ZnO in solid form. These particles get carried away by the counter current gas flow through the reactor and is collected in the baghouse. The residual solid phase at the end of the kiln contains all non-volatile metal oxides. This Waelz slag, is inert and can be used as filler material for construction.
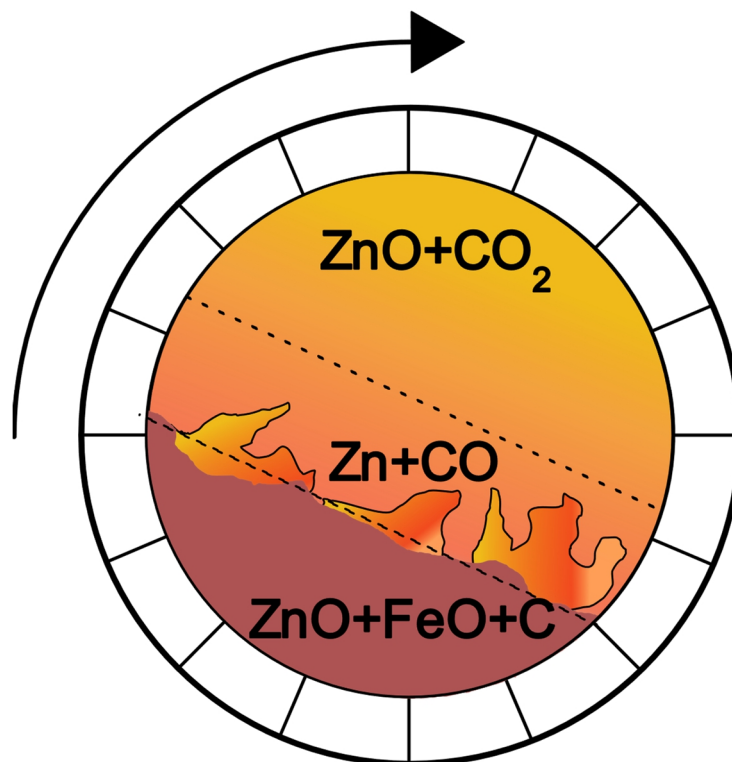

Figure 5: Schematic overview of the Waelz process, cross section of the rotary kiln [28, 29]

This process and others like it which focus on Zn, however, are not suitable for stainless steel dust [9, 10]. The problem hereby is that Cr, Ni, and others would end up in the resulting slag, from which an extraction would be difficult. Therefore, a variety of processes for retrieving Cr and Ni have been developed in the last decades, most of which are of pyrometallurgical nature. Table 3 gives an overview of the processes used for recovery of Cr and Ni from stainless steel dust, originating from the EAF. Hereby can be seen, that most processes are using carbon as reducing agent in combination with plasma furnaces. Furthermore, the recovery rates of those processes are satisfactory according to the found literature.

Table 3: State of the art for the recycling of stainless steel dust

Process	Applied technology	Reduction agent	Recovery rate		Literature
			η_{Cr} [%]	η_{Ni} [%]	
ScanDust	Plasma generator	Carbon	90	90	[16]
Enviroplas	Plasma generator	Carbon	92	96	[14, 15]
Inmetco	Rotary hearth furnace	Carbon	97	98	[12, 30]
Kawasaki Star	Shaft furnace	Carbon	90	95	[11, 31]
Iron bath process	Liquid Fe bath	Carbon/ferrosilicon	73	-	[32, 33]
Slag-Dust-pellets	Direct reduction	Carbon/ferrosilicon	91	92	[32]

3.1 Pyrometallurgical recycling

As previously mentioned, most of the processes for the recovery of valuable metals form EAF dust are carbon based and energy intensive processes. The following chapter will discuss those, which are applied in industry, as well as new developments in detail.

3.1.1 ScanDust

The dominant process in Europe to recover Cr and Ni from stainless steel dust is the ScanDust process from Befesa in Landskrona, Sweden. The concept of this process is the reduction of those residues by the means of plasma generators in combination with Carbon based reducing agents [16]. Like mentioned above in Table 3, this is a quite commonly applied technological approach for the recovery of such valuable metals. The yearly output of Cr and Ni bearing ferroalloy produced at the plant in Landskrona accumulates to about 70 000 t/year [34]. A schematic process flow sheet of the ScanDust process can be observed in Figure 6.
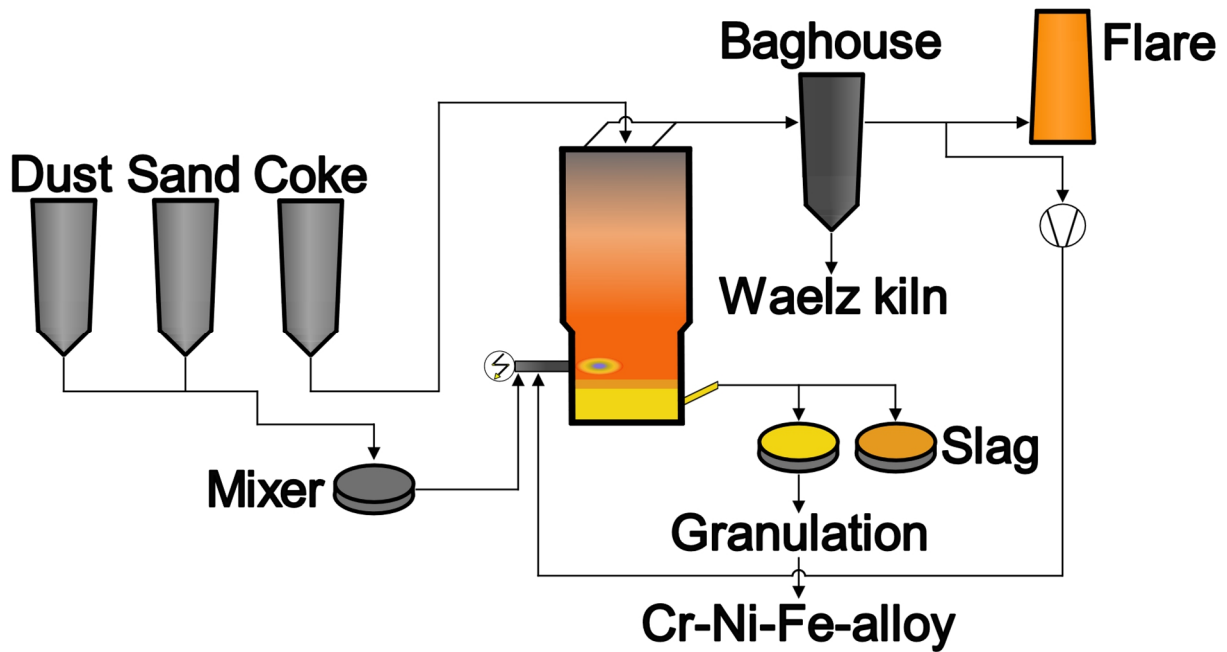
Figure 6:Process flow of the ScanDust process for the recovery of valuable metals [16, 34]

Before introducing the dust into the furnace, a blending step with sand occurs. This is performed to maximize the efficiency of the recovery of Cr and Ni during the process. Following this step, the mixture is transported to the furnace and injected via the plasma generators. In the intermediate area of these generators, the temperature reaches up to 5 000 °C and the metal oxides are reduced. The section of the furnace above the generators is filled with coke, which acts as reducing agent mostly in gaseous form of CO. The resulting Cr and Ni rich hot metal accumulates in the heart at around 1 500 °C, like in a shaft furnace. After a sufficient amount of hot metal amassed in the hearth, the furnace gets tapped. After tapping, which happens discontinuously, whenever enough has accumulated, the hot metal is transferred to a preheated tundish and granulated [16, 34].

Highly volatile elements like Zn and Pb are carried out of the reactor during the process and are being collected as oxides or in metallic form on their way to the baghouse. These Zn bearing dusts are then shipped to one company owned "Waelz" kiln and there treated to extract Zn form the dust [16].

3.1.2 Enviroplas

The Enviroplas process, developed by Mintek in South Africa, uses a graphite electrode in a converter to create a plasma-arc for the recovery of valuable metals from stainless steel dust. For this, the dust must be pelletized together with coke fines as well as silica and partially dried. This is done to assure that the dust is not carried over to the exhaust system. In Figure 7, the process outline and setup of the Enviroplas process can be observed. The furnace itself consists of a refractory lined cylindrical shell and conical roof. In the bottom of the vessel,

several steel rods are installed, which act as the anode to close the electrical circuit. The former mentioned graphite electrode acts as the cathode in the process which lights the electrical arc for the energy needed in the process [35]. Direct current is used for creating the arc. The resulting hot metal contains the metallic components and is tapped discontinuously at about 1 500-1 650 °C every two to three hours [15]. For Zn rich dusts, a lead splash condenser can be intercalated in the exhaust system before the baghouse [35, 36]. Such furnaces can process up to 30 000 t of stainless steel dust per year [14, 36].
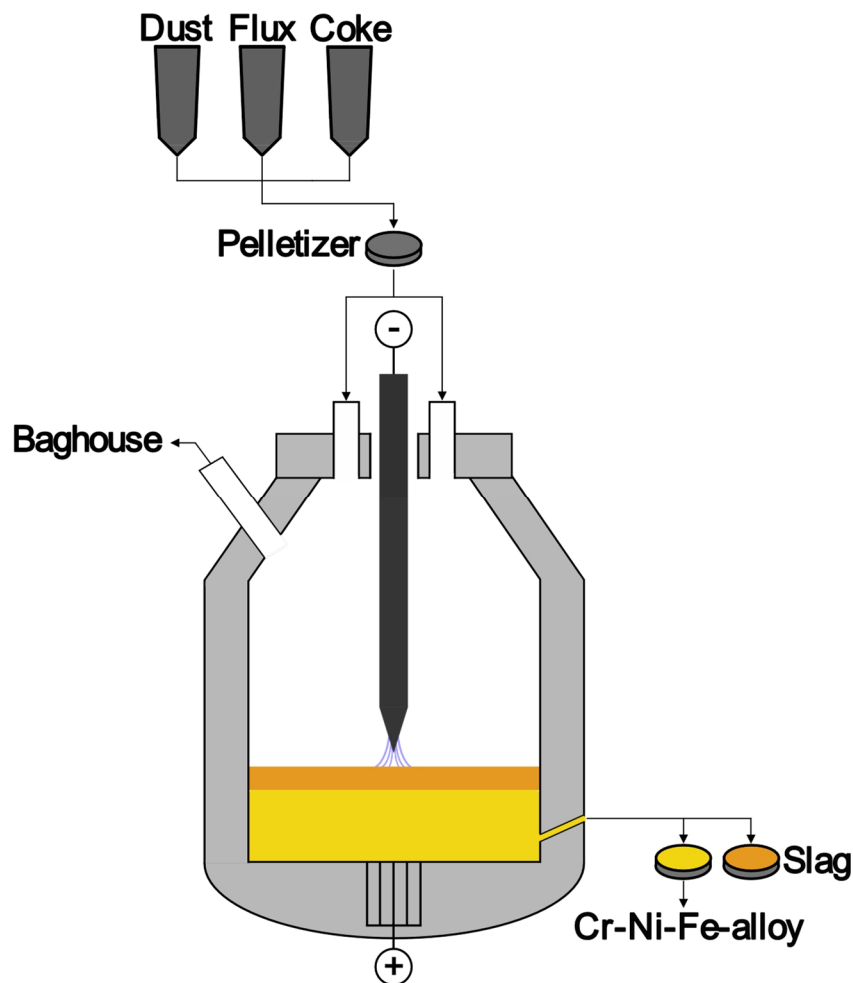

Figure 7: Depiction of the Enviroplas process [35, 36]

3.1.3 Kawasaki Star

The Star process, developed by Kawasaki (today JFE steel cooperation), uses a coke filled shaft furnace concept for the recovery of Cr and Ni. Hereby the coke is introduced via the top part of the furnace and moves downwards to the hearth. In the section above the hearth, two levels of tuyeres allow hot blast, which is produced by cowpers, access the furnace. In the upper level of the tuyeres, the dust is injected without prior agglomeration into the shaft furnace with an injection lance. In combination with the hot blast and the coke, a reducing atmosphere is produced, which reacts with the oxides in the dust and forms metallic components, which in

the case of Cr, Ni, and Fe accumulates in the hearth. This liquid ferroalloy is tapped together with the resulting slag discontinuously. Volatile metals like Zn and Pb can be obtained in the dust collected in the baghouse. For such operations, the top of the furnace has to have a temperature higher than 900 °C, to prevent the condensation of Zn and Pb [11, 31]. A schematic depiction of the Kawasaki Star process can be seen in Figure 8. The high coke rate of about 1 500 kg_{coke}/t_{alloy} can be seen as a disadvantage for an otherwise simple recovery concept compared to the plasma generator concepts. Shaft furnaces used in the Kawasaki Star process can recover up to 150 t_{alloy} per day [31].
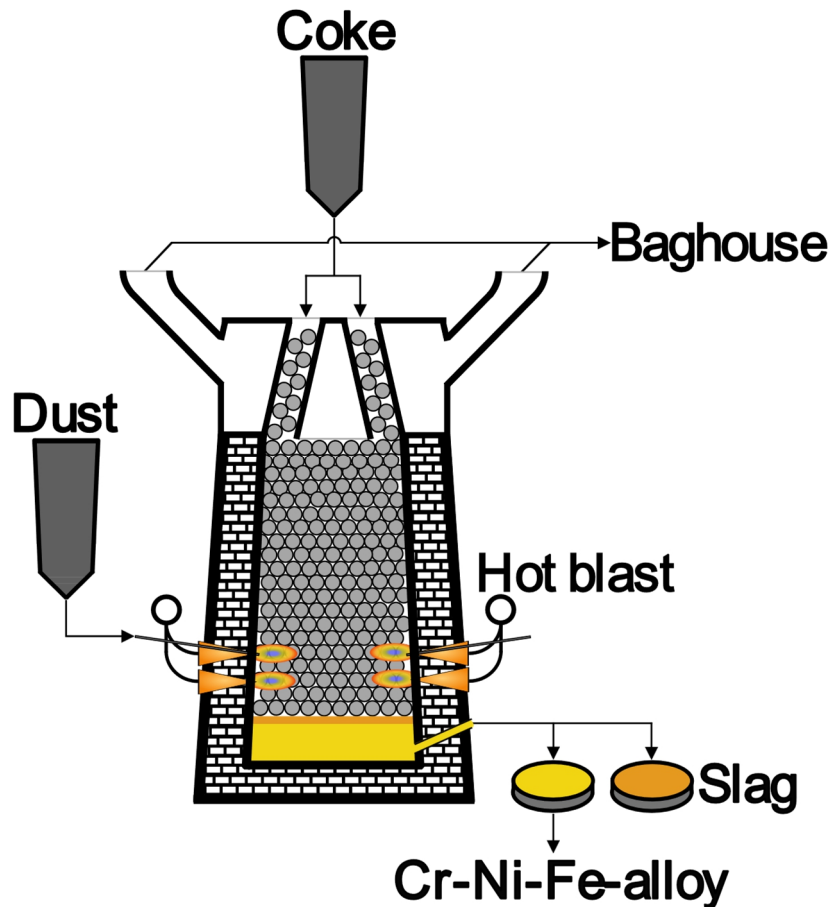

Figure 8: Schematic depiction of the shaft furnace used in the Kawasaki Star process [11, 31]

3.1.4 Inmetco

The Inmetco process consists of multiple stages, as can be seen in Figure 9. The first stage is to produce pellets consisting of stainless steel dust, coal fines or coke and water via a pelleting disk. These uniformly sized pellets contain enough carbon to be reduce the more noble oxides during their stay in the rotary hearth furnace [17]. The hearth of the furnace rotates slowly, while a thin layer, about one to three pellets thick, of previous dried pellets is introduced into the furnace. During their stay in the burner heated furnace, the pellets begin to partially metallize through reactions between the oxides with the reducing atmosphere as well as the

carbon carrier in the pellets themselves, beginning with Fe and Ni. After nearly a full spin on the hearth, the pellets are being extracted and introduced into an EAF, where the rest of the oxides like Cr are reduced to their metallic form. This constitutes the last step of the Inmetco process for the recovery of valuable metals. The product is similar to all previously mentioned a ferroalloy. If the dust contains volatile components like Zn-oxides, they are reduced in the rotary hearth and recovered through the baghouse filters. With one of these plants yearly 47 000 t of waste can be recycled [12, 17, 18, 30].
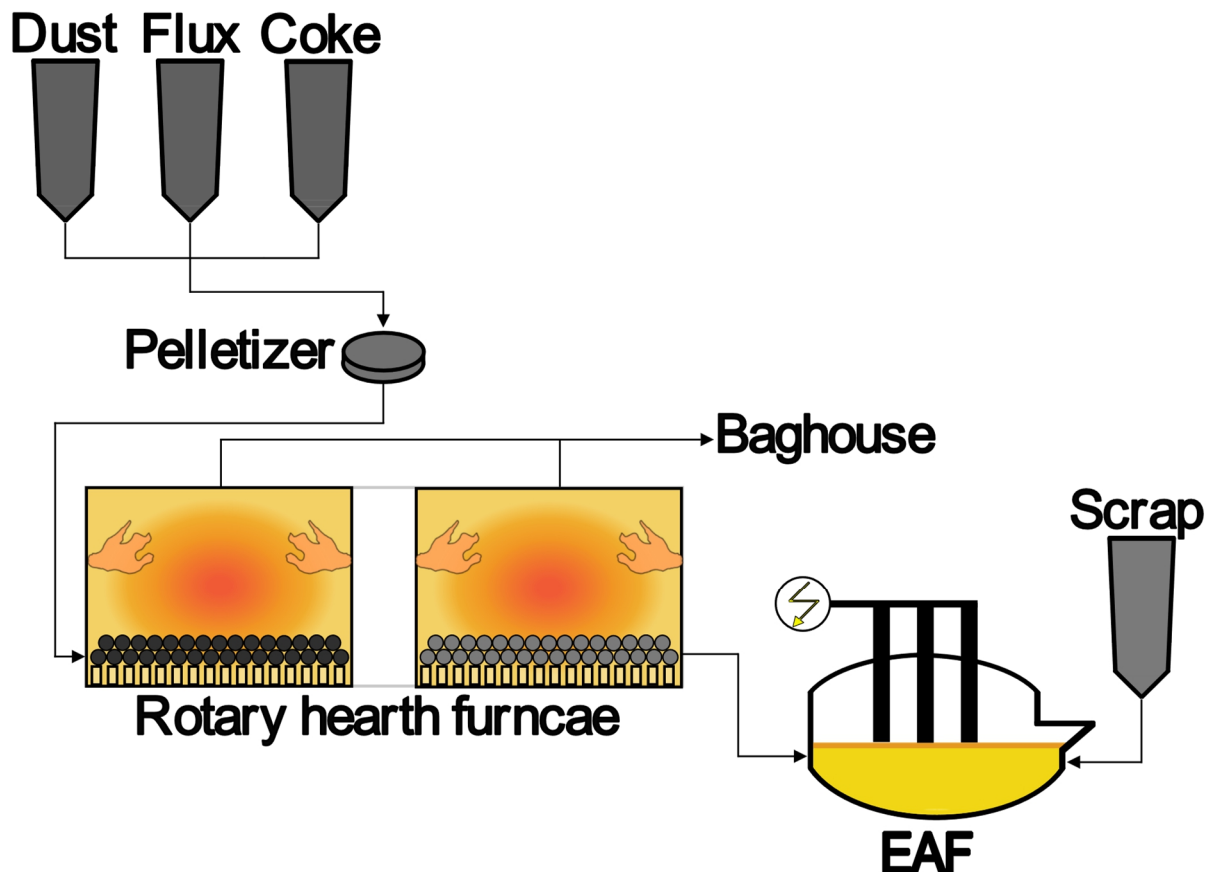

Figure 9: Schematic overview of the Inmetco process [12, 30]

3.1.5 Experimental pyrometallurgical processes

The recovery of Cr through self-reducing dust-slag pellets was proposed by Liu at al. [37]. Hereby the two Cr containing residuals are being mixed with coke and afterward heated up to 1 400 °C in an Ar stream. During heating and the holding period, the Cr-oxides are directly reduced by the carbon. Through this, recovery rates over 90 % can be achieved [37].

Drissen et al. investigated the effect of the recovery of Cr by blowing stainless dust via lances into the slag of an EAF [38, 39]. Like with the Fe-bath processes, an addition of FeSi supported the recovery of Cr into the stainless steel melt [38].

Another process for recovering Cr and Ni from EAFD is the from Cyro et al. proposed process of pelletizing the dust with either carbon carriers or FeSi with subsequent immersion in a cast

iron bath. For FeSi experiments high recovery rates could be obtained [32]. Zhuo et al. proposed a similar idea for the recovery of Cr and Ni [33].

3.2 Hydrometallurgical recycling

Nevertheless, hydrometallurgical solutions can offer a more energy efficient, economic, as well as ecological way of recovering valuable metals from EAFD, only a hand full of concepts have tried it. Most of these focus on the recovery of Zn from EAFD rich in Zn [25, 40, 41]. A method found in literature to extract Zn from AOD-sludge, was by alkaline leaching in NaOH, whereas Zn was dissolving to a satisfactory extend, while practically no dissolution of Cr, Ni, and Fe occurred [25]. Aromaa et al., used the same leaching agent as well as H_2SO_4 for the selective leaching of Zn from stainless steel dust and found similar results for NaOH [41]. For H_2SO_4, they found out, that even at lower temperatures Zn and Mo were dissolved quite good as well as that Ni and Cr could be leached by it, but only in a range of a few percent [41].

Although the extraction with the sole aim of dissolving Cr and Ni by hydrometallurgical means have not been found in studies, Majuste et al. tried to dissolve Fe from AOD-sludge, which can be similar in composition to EAFD [23, 42]. In this study, 12 vol-% HCl was used to determine the leachability of Fe from the dust. The conclusion was that not only Fe was leached by this solution, but also significant amounts of Ni and Cr could be proven to be dissolved [42].

4   Characterisation of EAF dust

The following chapter will summarize the characterisation done for the dust investigated in the course of this thesis (EAFD_1). First the morphology was analysed with a scanning electron microscope (SEM) (JOEL JSM-IT300) as well as a rough elemental analysis was gained through energy-dispersive X-ray spectroscopy while the sample was in the SEM. This rough analysis, together with data from literature, was the base for the requested analysis of the sample, which was sent to a subcontractor for elemental analysis. Furthermore, a X-ray-diffraction (XRD) pattern was measured for a qualitive analysis of the phase distribution. This was done to have a basis for later thermodynamical calculations regarding leachability of individual compounds of the dust. The final step of the characterisation was the measuring of the loss of volatile components via thermogravimetry analysis (TGA).

Initially eight different EAFD were sampled at stainless steel producers and characterised for their usage in the leaching experiments. For simplicity and not to overextend the thesis, the author chose only to go into the detailed characterisation of the chosen dust. The steel is produced via the former explained EAF route and then refined in an AOD converter or VOD ladle treatment and finally casted via horizontal continuous caster or ingot caster [19]. Together with other more specialised process routes, the steel plant produces about 145 000 t_{Steel}/year, which accumulates roughly to an amount between 1 450 to 2 900 t of dust a year [3].

4.1 Morphology

The morphology of an EAFD often varies from melt to melt, similar to the elemental analysis. Nevertheless, an analysis of the morphology can give an important insight into the composition and distribution of different elements and therefore corresponding phases in the dust. An array of the morphology can be observed in Figure 10, which displays different magnification SEM-images. In Figure 10 (a), a general overview of the dust, which adheres to the graphite layer of the stamp, can be seen. A wide array of smaller and larger dust particles can be seen, whereas the smaller outnumber the larger. Figure 10 (b) portrays an agglomeration of different sized particles. In parts (c) and (d), with increasing magnification, smaller particles with a size under 50 µm can be seen in the background of the lager particles. In Figure 10 a to d, the tendency of the formation of spherical shaped dust can be observed, which is in line with literature. As mentioned above, particles size of the dust can often be under 25 µm, which can also be seen in the SEM-Images below [6].

A pre-chemical analysis was performed with the SEM, by scanning larger areas like Figure 10 (a) with the integrated EDX-sensor. This was necessary, like mentioned above, to

predetermine roughly elemental contents. Further chemical analysis will be discussed in chapter 4.2.
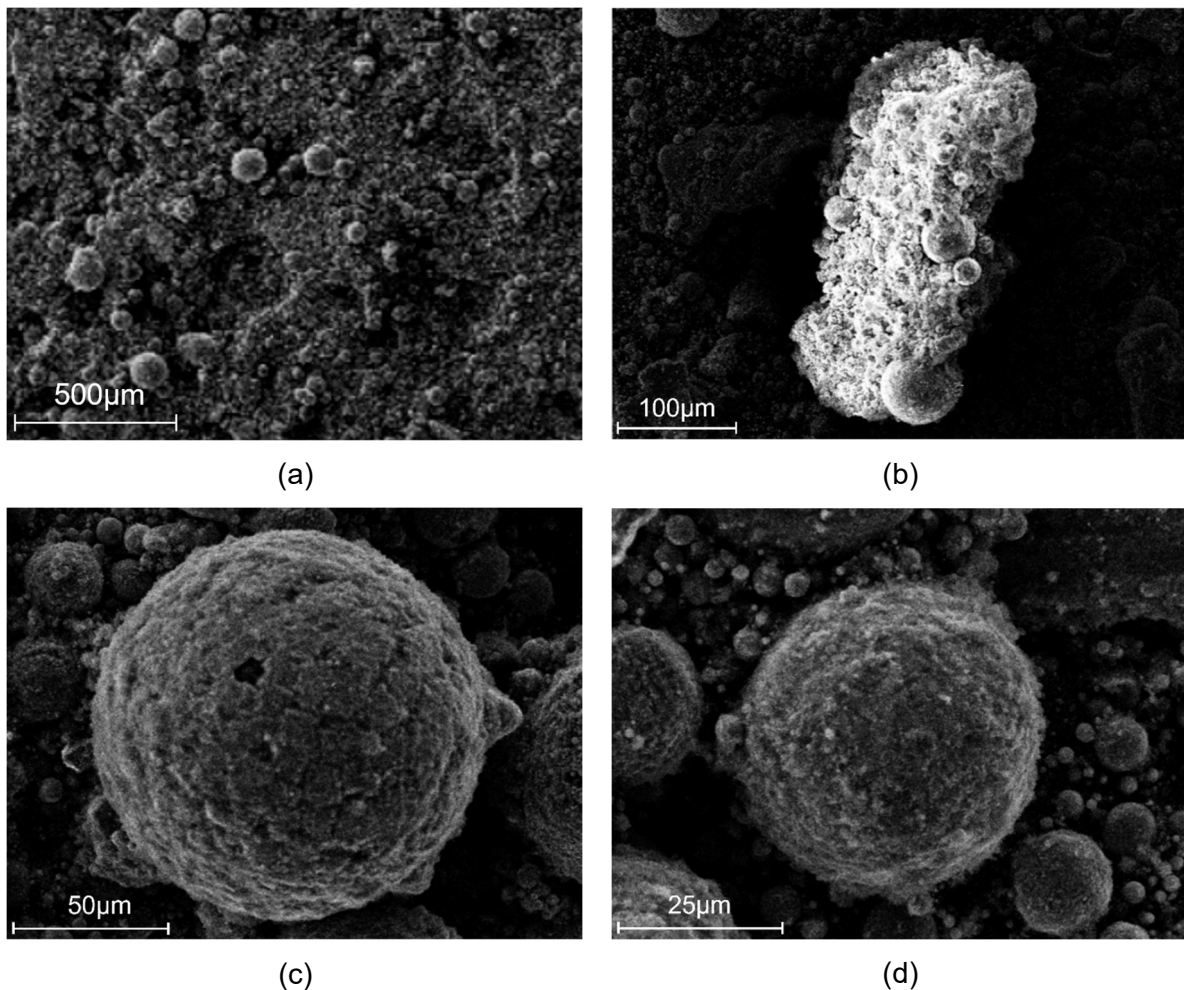

Figure 10: SEM-Images of increasing magnification (a to d) of EAFD_1 on a graphite layered stamp

4.2 Chemical analysis

As a basis for all further experimental steps, a chemical analysis was conducted by sending a representative sample of 10 g to "A.M.C.O united sampler and assayers GmbH" in Duisburg, Germany. There the samples were prepared accordingly for measuring and the analysis was performed with the in Table 4 mentioned methods for the corresponding elements listed. The first, "DIN EN ISO 11885, 2009-09", uses inductive coupled plasma optical emission spectroscopy (ICP-OES) for the metals listed in Table 4. This standard describes a process to determine low contents of metals (< 2 g/l) in different bodies of water (drinking, waste, raw and ground water) as well as for sludges and sediment and their chemical pulping [43]. Furthermore it is a valid way of measuring contents of other material, which is chemically extracted [43].

Table 4: Used method for analysing each element

Used norm	Elements
DIN EN ISO 11885, 2009-09	Al, Ca, Co, Cr, Fe, Mg, Mn, Mo, Ni, Si, V, W, Zn
DIN EN 14582: 2016-12	Cl
DIN 38405 Teil 1 : 1985-12	F

Both "DIN EN 14582: 2016-12" and "DIN 38405 Teil 1 : 1985-12" describe the characterisation and measurement of halogenic contents of either residues for "DIN EN 14582" or for different bodies of water in the case of "DIN 38405" via different chemical methods [44, 45].

The results of the elemental analysis can be observed in Table 5 for EAFD_1, which was ultimately chosen for experiments for its high content of Cr and Ni.

Table 5: Chemical analysis of EAFD_1

Elements [%]					
Al	0.70	Ca	1.25	Cl	0.27
Co	0.33	Cr	6.6	F	0.10
Fe	55.4	Mg	0.28	Mn	0.41
Mo	1.3	Ni	4.5	Si	0.28
V	0.20	W	0.18	Zn	0.20

Table 6 represents the range of the analysed elements of all eight dust. Here the high fluctuation of the elemental content can be observed.

Table 6: Range of elements present in the different characterised EAF dusts

Elements [%]					
Al	0.17-1.0	Ca	1.25-10.8	Cl	0.1-0.67
Co	0.01-0.33	Cr	1.3-6.6	F	0.1-1.0
Fe	15.6-55.4	Mg	0.28-8.6	Mn	0.41-3.1
Mo	0.04-1.3	Ni	0.04-4.5	Si	0.28-8.9
V	0.02-0.2	W	0.01-0.18	Zn	0.2-36.2

A comparison of the elemental analysis for the metals Fe, Zn, Cr, and Ni can be observed in Figure 11 and Figure 12. In these bar charts, the content of Fe and Zn can be seen as for most of the analysed dusts are nearly at a level above 20 % for Fe and 15 % for Zn. As mentioned above, the desirable elements for reprocessing are Cr and Ni. When comparing these elements in Figure 12, it can be seen, that EAFD_1 is the only dust with high concentrations of both Ni and Cr and simultaneously low contents of Zn.
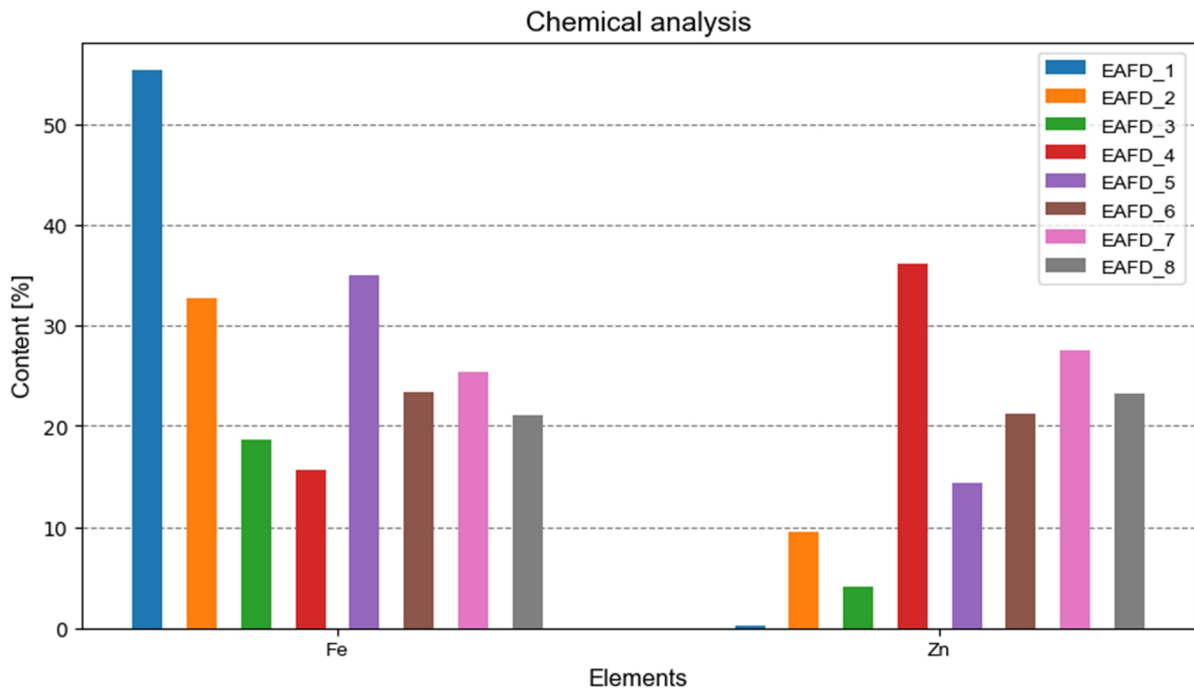
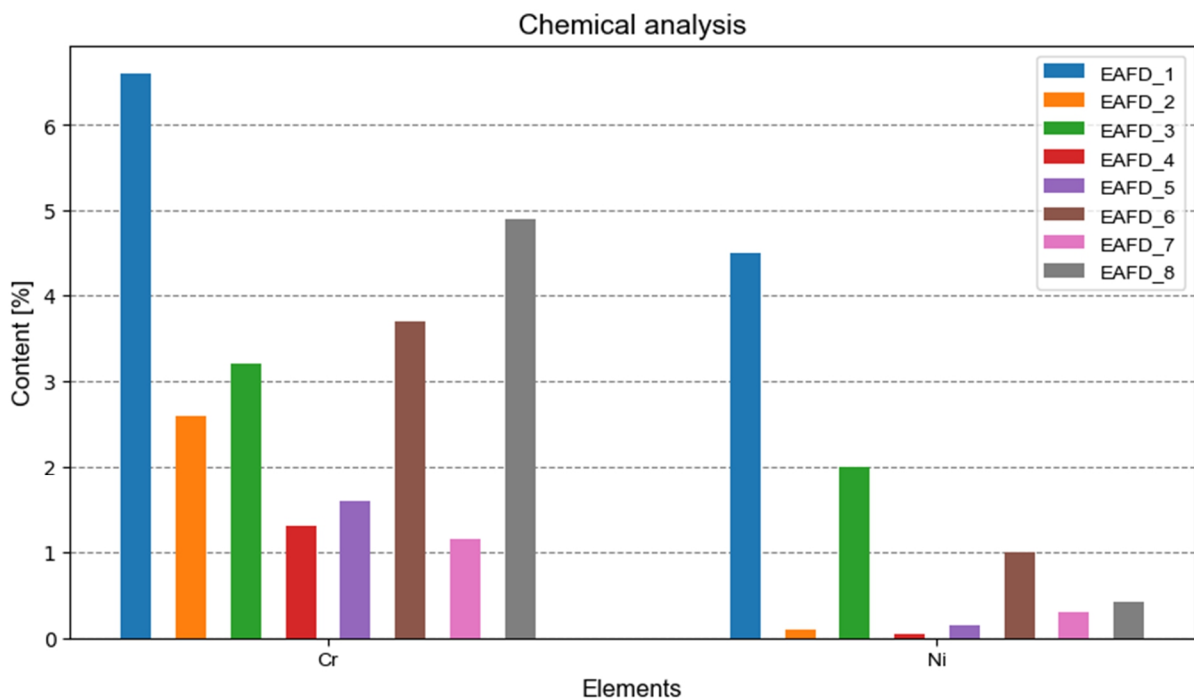Figure 11: Fe and Zn content of all analysed dusts

Figure 12: Cr and Ni content of all analysed dusts

4.3 X-ray diffraction analysis

The data of the XRD-analysis performed can be seen in Figure 13. The measurement was performed by the "Material Centre Leoben", a scientific research institute situated in Leoben. For analysis of the data, the program Match!3 version 3.16 in combination with the

crystallography open database (COD) version from 05.12.2023 were used to process the measured data and corresponding phase identification [46, 47]. Before the peak analysis, the raw data was smoothed via Match!3 integrated feature. After processing, elements contained in the dust had to be chosen by clicking on them, whereas afterwards, the program tried to match the peaks with fitting phases. The matching had to be done by hand, by choosing the phase, which had the highest figure of merit at the peak position. Following that procedure, some of smaller identified peaks, could not be attributed to a phase. Moreover, the significantly noticeable background could be a result from slag bearing particles, which solidified fast into glass like structures.
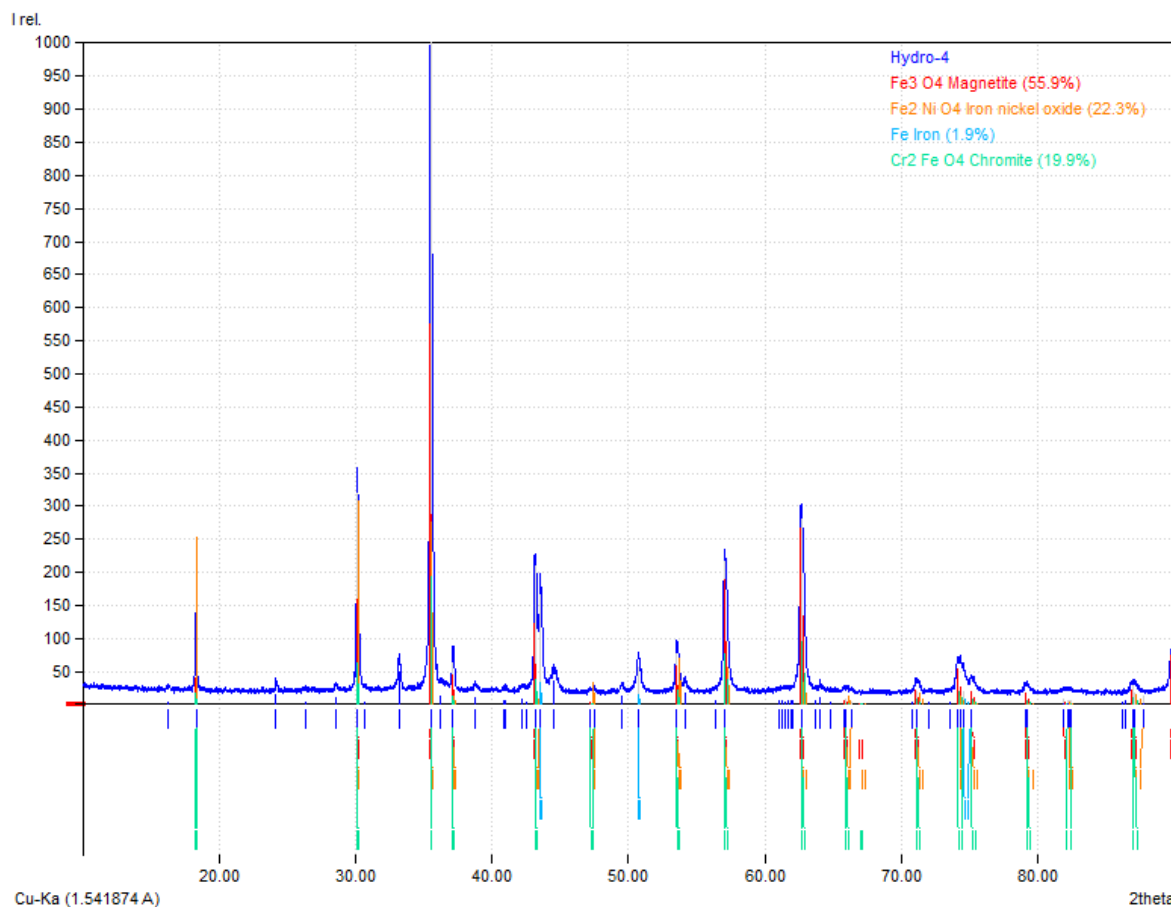
Figure 13: Full data of XRD-Analysis of EAFD_1 with peak identification [46]

As can be seen in Figure 13, the dust mainly consists of Fe-spinel phases which contain the main alloying elements Cr and Ni. Because of that and the relatively vicinity and often overlaying and resulting broad peaks of the different spinel phases, the identification of the phases related to a certain hardship, as is also reported in literature [23]. After the main phases were determined, a metallic Fe phase could be found. The appearance of small Fe droplets was also observed visually when handling the dust in the leaching experiments. These appeared as shining metallic spheres.

4.4 Thermogravimetric analysis

The thermogravimetric analysis was performed with a "Netsch STA 409". The parameters investigated can be observed in Table 7, where flow rates of the process gases used in the experiments, heating rate, holding time as well as maximum temperature are displayed.

Table 7: Experimental parameters of the thermogravimetry analysis

Gas flow rate [Nl/min]	Max. Temperature [°C]	Heating rate [°C/min]	Holding time [min]	Process gas
0.25	1400	10	30	Syn. Air/Ar

Before the analysis can be performed, the masses of the crucibles as well as the investigated sample must be determined. These masses can be seen in Table 8.

Table 8: Weight in masses of crucibles and sample

Experiment	Reference crucible [mg]	Sample crucible [mg]	Sample [mg]
C1	1459.45	1462.45	100.04
C2	1459.13	1461.95	100.35

Figure 14 (a) and (b) both represents the data of thermogravimetric analysis of EAFD_1. In both diagrams beginning from room temperature up till 1 400 °C, a loss of mass can be detected. The constant loss till about 400 °C of volatile phase does not show change their slope and can thus be considered one single component, which evaporates. For both samples, this loss is about 0.5 % of the overall mass. In this temperature range the evaporation of H_2O in its surface and various chemically bonded form takes place. Since the same can be observed in Ar atmosphere as well as in synthetic air, this is the most likely volatile phase which evaporates. In the temperature range beginning at 400 °C up to 1 000 °C a gain of mass can be detected in Figure 14 (a), which at 750 °C the data in (a) shows that a second reaction takes place, which could be the oxidation of Zn and subsequent evaporation of Cl form the $ZnCl_2$. This is indicated through the change in the steepness of the slope in this temperature range. The total mass gain of about 8 % in synthetic air can be attributed to the oxidation of metallic Fe, which was identified in the XRD-analysis as well as the oxidation of the former mentioned Zn. This mass gain is completely absent in the experiment conducted with Ar, which indicates that this is most likely a oxidation reaction. For the mass loss in (b) between 400 and 800 °C no phase could be identified with the data available. A distinctive loss between 750 °C and 1 000 °C can be observed in (b). This can be attributed to the evaporation of $ZnCl_2$ at these temperatures, which would be the most thermodynamically stable chloride in the absence of Na. This loss of about 1.5 % of the mass correlates with the amount of both

elements in the dust. The in Figure 14 (c) depicted diagram represents the heating rate and holding time during the experiment.
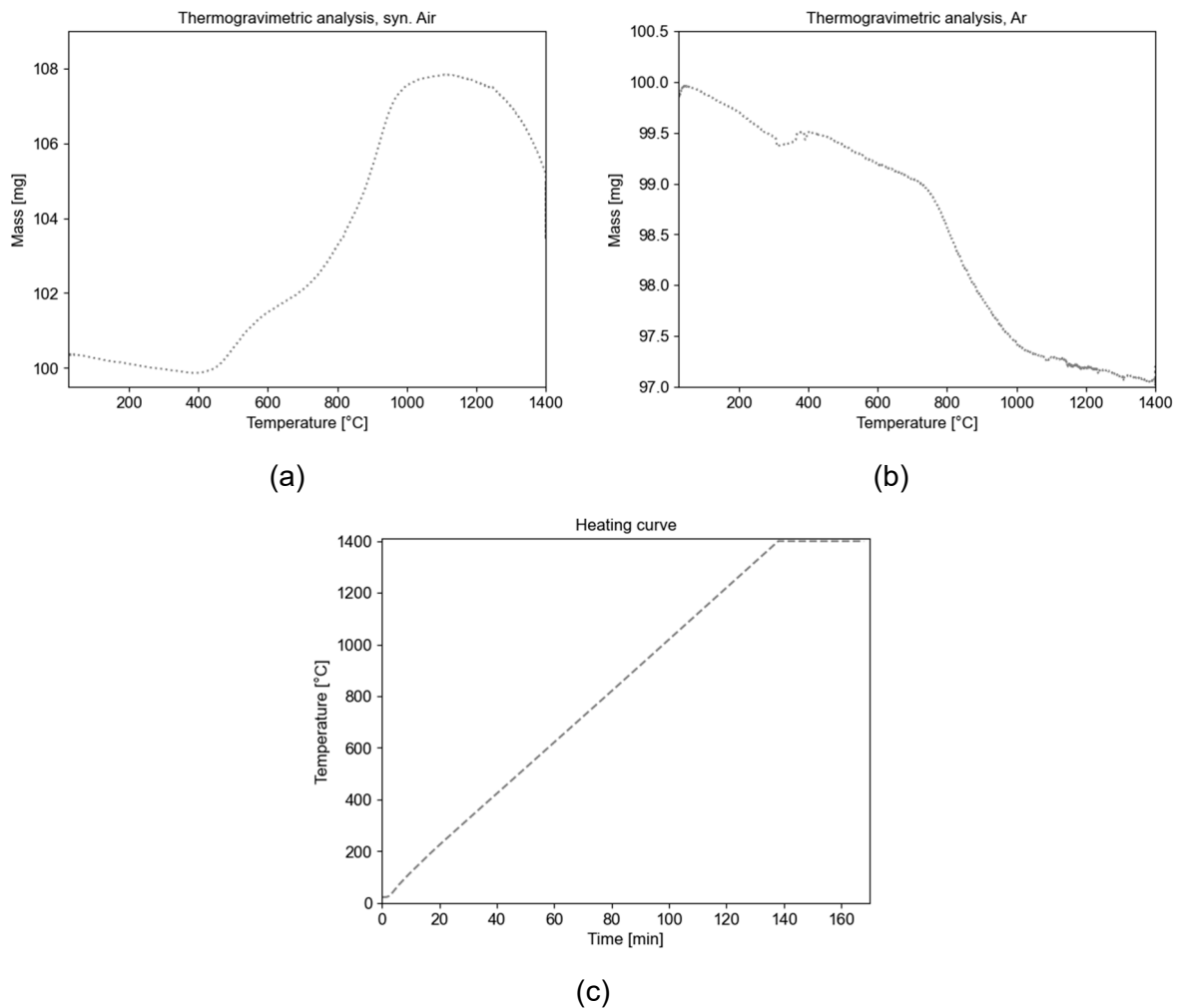

Figure 14: Thermogravimetric analysis of EAFD_1, (a) synthetic air C1, (b) argon C2, (c) experimental temperature-time curve

4.5 Summary

As explained in this chapter, EAFD_1 was chosen for the first series of experiments of the following reasons. Compared to other dusts, EAFD_1 offers high contents of Cr, Ni and Fe and especially low concentration of Zn. This might be an indicator, that low amounts of Zn-coated scrap were used in its production, therefore it can be assumed that high quality steel scrap was remolten in the EAF. Figure 14 shows that EAFD_1 also contains a low amount of volatile phases. The combination of the consistency within the chemical, XRD-analysis as well as calculations of the theoretical phase distribution based on phases present according to literature was a major factor for deciding for EAFD_1. The phases identified in the dust via the XRD-analysis can be seen in Table 9. These are in unison with previous mentioned literature

[7, 8, 22, 23, 25]. Furthermore, the reasonable and sufficient amount of dust, which was about 2.5 kg before the experiments, was also an aspect for taking a decision to choose EAFD_1.

Table 9: Identified phases in EAFD_1

Phase name/chemical composition			
Iron-chromium-spinel	$FeCr_2O_4$	Nickel-iron-spinel	$NiFe_2O_4$
Magnetite	Fe_3O_4	Iron (metallic)	Fe

5   Leaching of EAF-Dust

As core of this thesis as well as that of the former mentioned project "HydroStäube", the design and implementation of a viable hydrometallurgical process, specifically the leaching step, is in the focus. For the propose of developing such a hydrometallurgical process, multiple leaching experiments have been conducted and out of the knowledge gained two optimized experimental setups, which can be seen in Figure 19 and Figure 23, have been developed. Furthermore, for finding suitable experimental parameters for the leaching of the previous analysed phases, thermodynamical calculations have been with the program HCS 10 form Metso Outotec.

5.1 Thermodynamic calculations

As mentioned above, to determine the desired pH-vale for the decomposition of the phases present in the dust, thermodynamical calculations regarding the stability of certain identified phases have been performed. The "equilibrium calculation" mode of HSC 10 was chosen to perform all those calculations, in which H_2O was the main component in the aqueous phase. The amount of H_2O is not visible in any of the calculated stability diagrams because of the relative high amount compared to the other species. Otherwise, this would lead to squeezing of other curves, which would have made a valid interpretation of the diagrams more difficult. Resulting products from the reaction of the addition of acids in H_2O, like H^+ and Cl^- for HCl, were added into the same phase as water and stet to the "Aqua" mode for the computation. These curves, which represent the corresponding ions, were dashed to distinguish them better from other species. Mineralogical phases and their resulting products were added in a separate phase for the calculation. In 400 steps 0.1 kmol of acid was added to the phases, which resulted in the diagrams. For all diagrams a temperature of 50 °C and seven iteration steps were used as basis. On the x-axis, the pH-value can be observed, which is limited to values between 2 and -0.5. The y-axis presents the equilibrium amount of the species in the diagrams. In Figure 15 the dissolution of chromite ($FeCr_2O_4$) in HCl can be observed, which takes place even at relatively high pH-values. Mostly the Fe in the phase dissolves at this point, whereas the Cr is not dissolved and accumulates in the Cr_2O_3 phase. When reaching pH-values under 1, Cr_2O_3 begins to dissolve and at around 0.3 all Cr is in solution. This means Cr_2O_3 not thermodynamically stable under a pH-values of 0.3.
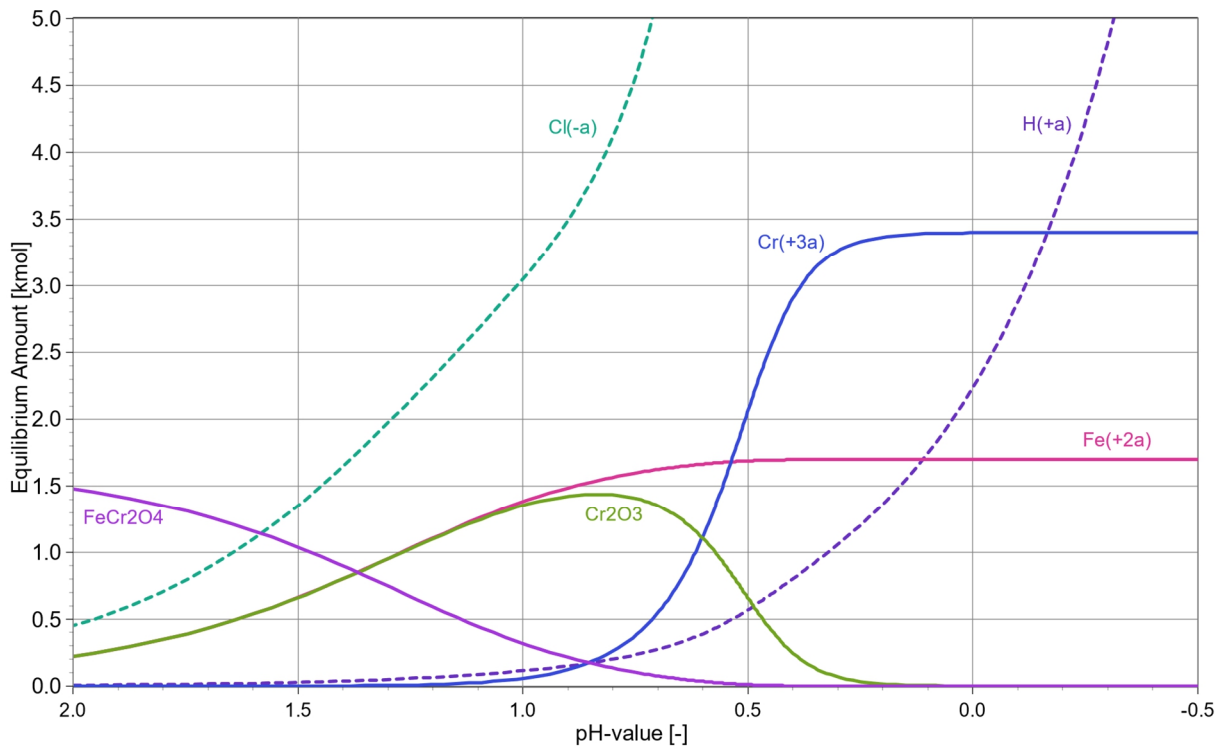
Figure 15: Thermodynamic calculations of the decomposition of chromite in HCl [48]

Figure 16 describes dissolution of a $NiFe_2O_4$ in HCl containing medium. Similar to Figure 15, the spinel phase is not thermodynamically stable at lower pH-values. Therefore, as mentioned above, should the experiments be conducted within the range of these conditions.
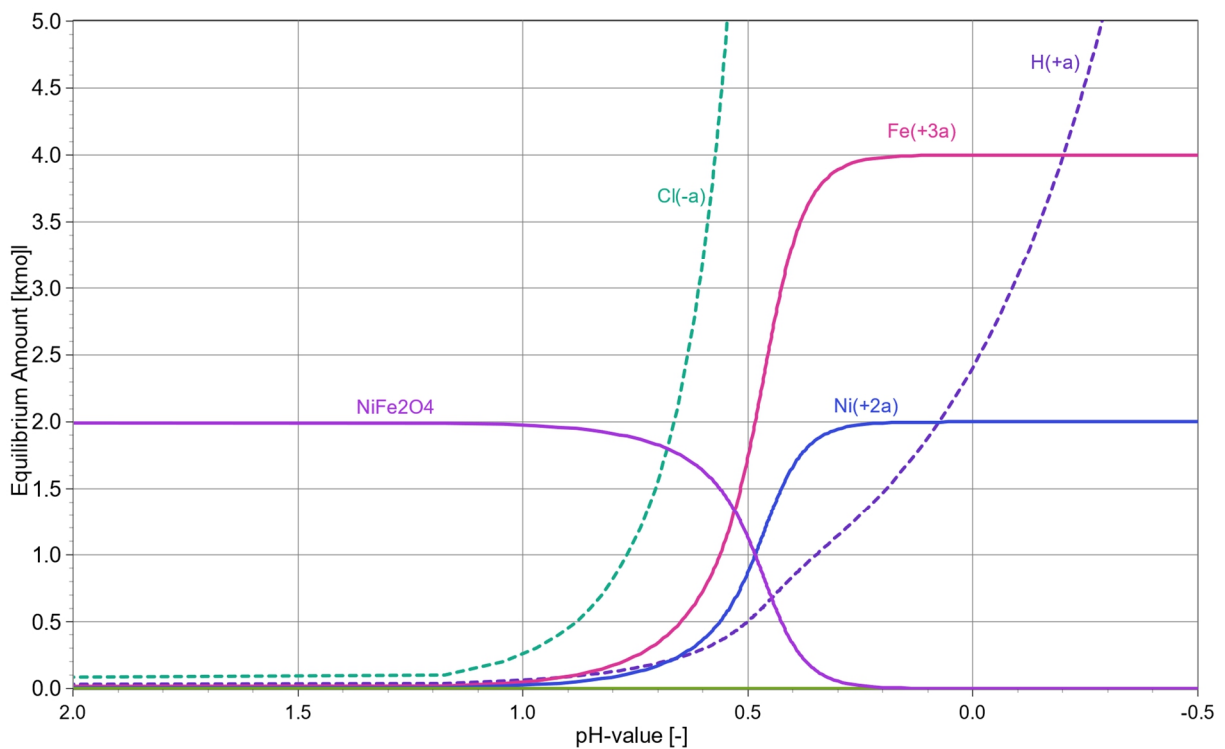

Figure 16: Thermodynamic calculations of the decomposition of nickel ferrite in HCl [48]

5.2 Tentative Experiments

The initial tentative experiments in course of this thesis were conducted to identify a suitable setup as well as to get the first set of resilient data for feasible parameters for planning of follow-up experiments. By finding some limitations of the assembly and interaction of the lab equipment, two improved setups for future experiments were developed. Both setups will be discussed in greater detail in this thesis at a later point in chapters 5.3.2 and 8.

5.2.1 Experimental parameters

For practical use and comparison, hydrochloric and sulphuric acid were used in these experiments. This is because of their widely usage in industry, common availability on markets, as well as their price, compared to other more expensive options. The temperature was limited to 60 °C to avoid excess vaporization of the leaching liquid. A solid to liquid ratio (S:L) of 1/10 was chosen, as is also quite usually for experiments this size according to literature. All these parameters are listed in Table 10 to provide an overview of the experiment as well as comparison to later experiments. A lower pH-value as calculated was chosen for these experiments for safety reasons, to prevent excess formation of hazardous gas evolution.

Table 10: Experimental parameters of the tentative experiments

Experiment	Acid	pH [-]	S:L [g/ml]	Temperature [°C]	Time [min]
T1	HCl	1	1:10	60	60
T2	H_2SO_4				

5.2.2 Experimental setup

As the setup used for these experiments, is quite basic, though it was intended for low leaching temperature. In Figure 17 it can be observed that a beaker is used as reaction vessel and the leaching suspension is stirred by a magnetic bar, which was agitated by the heating and stirring plate underneath the beaker. The temperature was controlled and regulated with a thermostat, which was in the leaching liquid all time and connected to the heating plate. To prevent the leaching of the thermostat, it was placed in a glass tube which itself was filled with silicon oil for better thermal conductivity. After the mixture of deionised water and EAF dust reached the desired temperature, acid was added via a dropping funnel until pH-value was in the pre-defined margin. The complete procedure of the experiment can be seen in Figure 18.
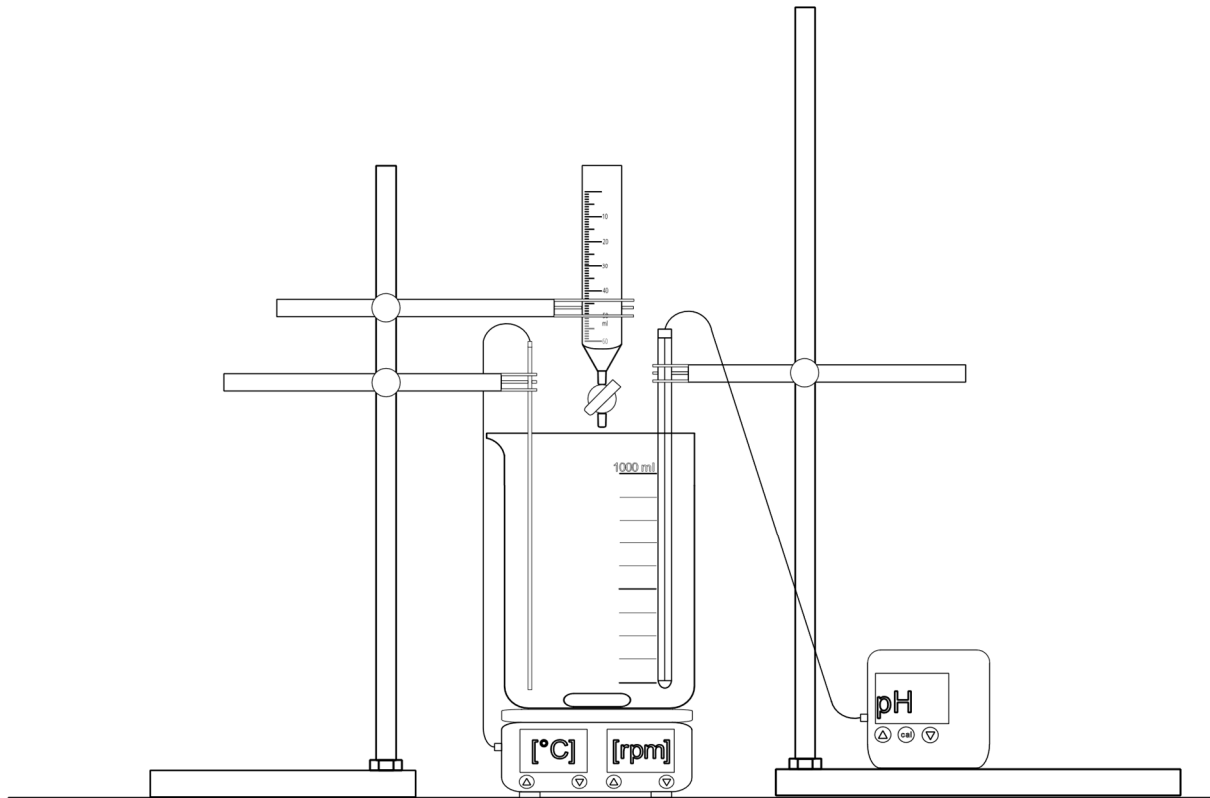
Figure 17: Experimental setup of the tentative campaign

For the duration of the experiment, the pH-value and temperature were kept at a constant value. After the completion of the experiment the slurry was filtered with an Büchner funnel and Erlenmeyer vacuum flask, which was connected to a water jet pump. This pump created an under pressure to separate the filtrate and the solid residue, which was held back via a filter paper. After the solid residue was removed from the Büchner funnel it was placed on a watch glass and put into the drying oven at 105 °C for at least 24 h or until the weight was constant. After this the solids and liquids were sent to the company A.M.C.O. for chemical analysis.
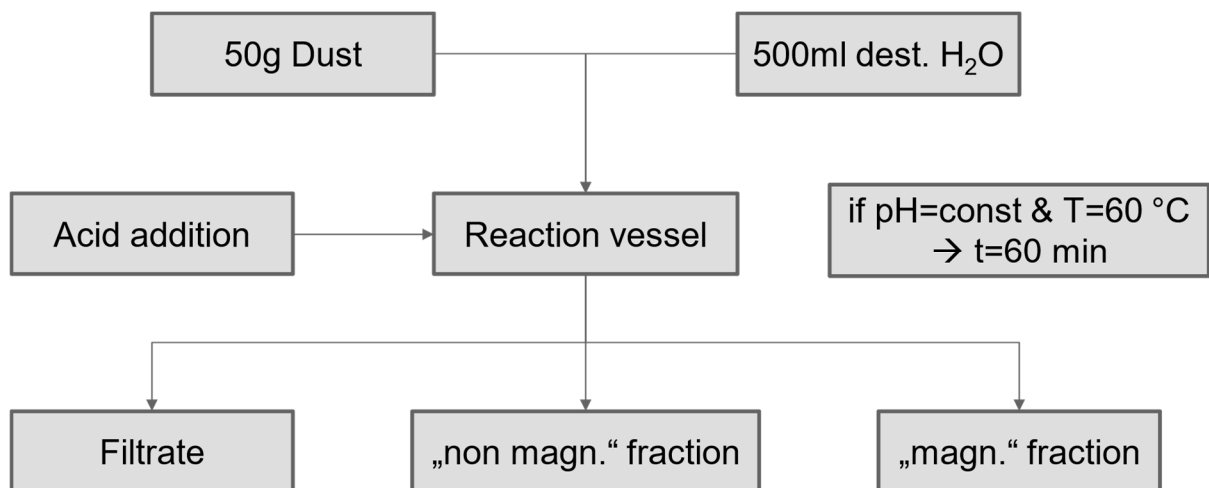
Figure 18: Flow sheet of the tentative experiments

5.3 Acid variation campaign

The aim of this campaign was to classify different acids and rank them for their use as a leaching and extraction agent for further experiments the in course of the project. For doing so, an analysis of the extraction rates of the previously defined valuable metals with each of the acids was performed after the experiments. The most promising acid would be used to conduct future parameter variation experiments.

5.3.1 Experimental parameters

As can be seen in Table 11 five different acids were investigated in these experiments. With the strong acids like hydrochloric (HCl), sulphuric (H_2SO_4) and nitric acids (HNO_3) the goal was to hold the pH-value of 0.3 during the leaching. This was determined by the thermodynamical calculations conducted in chapter 5.1. Because the organic acids possess a pK_a-value of 4.75 for vinegar acid (CH_3COOH) and 3.13 for citric acid ($C_6H_8O_7$) a pH-value of lower than 2.4 and respectively 1.75 was not reachable.

Table 11: Experimental parameters of the acid variation campaign

Experiment	Acid	pH [-]	S:L [g/ml]	Temperature [°C]	Time [min]
A1	HCl				
A2	H_2SO_4	0.3-0.5			
A3	HNO_3		1:10	60	60
A4	CH_3COOH	<2.5			
A5	$C_6H_8O_7$	<2.5			

The dilution for each of the used acids is listed in Table 12. Most of the acids could be used without addition of water, only H_2SO_4 and $C_6H_8O_7$ had to be mixed with deionised H_2O. Though sulphuric acid at 96 vol-% is liquid, it was not possible to add the acid via the syringe system, because of its high viscosity. Citric acid was only available in solid form and therefore had to be added to water to create the acid used in the experiment.

Table 12: Added acids and their respective dilution in vol-%

Acid	Dilution with deionised H_2O [vol-%]
HCl	32.0
H_2SO_4*	48.0
HNO3	40.0
CH_3COOH	100
$C_6H_8O_7$*	43.5

*had to by diluted by hand

Citric acid and vinegar acid were chosen in these experiments to investigate the effect of organic acids for researching the potential of bio leaching experiments and further use of them. Also, a pretreatment with vinegar acid is a promising step to dissolve free CaO in the dust.

5.3.2 Experimental setup

As can be seen in Figure 19, the experimental setup of the tentative experiments has changed to counter the problems encountered during the first trials. The magnetic bar that was used to stir the leaching solution was substituted by a glass stirrer which is attached to an agitator. This completely prevented the build-up of magnetic fraction on the stirrer completely. For better control of acid feed and therefore resulting in a better control of the pH-value, a disposable syringe was used. Before each of the experiments the dead volume of the connecting flexible tube had to be determined. Thus, using this system a continuous acid feed could be established, and the pH-value could be held easier in a constant range. All those improvements led to a more complete mass balance as well as easier handling of the filtering operation after the experiment.
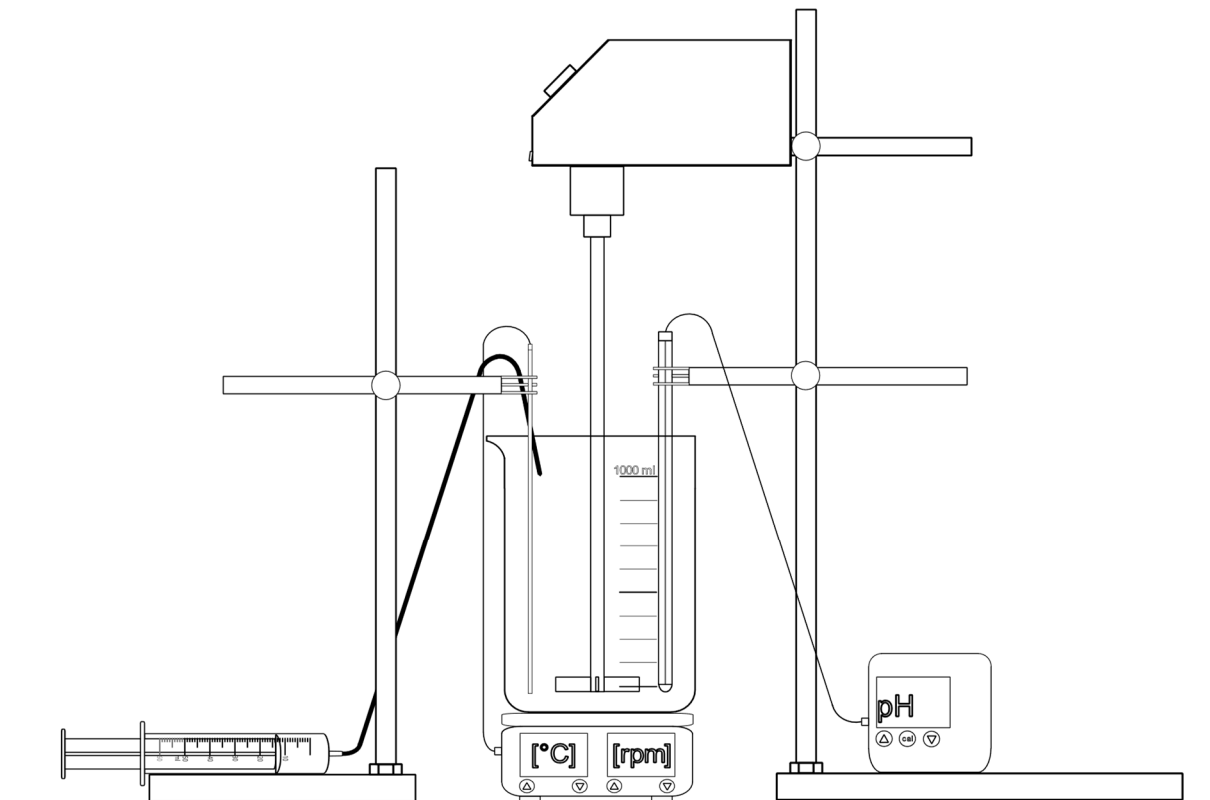
Figure 19: Experimental set up of the dust leaching

After assembling the portrayed lab equipment as shown in Figure 19, 50 g of EAF-dust was weight, and 500 ml of deionised water measured with a measuring cylinder, to be mixed in the beaker. Simultaneously the agitator as well as the heating plate was switched on to keep the particles suspended and the temperature constant. After reaching the reaction temperature,

as is portrayed in Figure 20, the acid was added to the beaker via the disposable syringe via the attached flexible acid resistant plastic tube. This was done until the pH-meter measured the desired and pre-defined value, after which the timer for the reaction time started. During the experiment the pH-value was kept constant and if necessary, some drops of acid were added via the syringe. After 60 min all the instruments which were in the leaching liquid were removed and the suspension was poured into a Büchner funnel with filter paper lining. The liquid was separated and dropped into an Erlenmeyer flask which was connected to a water jet pump which applied an under pressure for the operation. After the filtrate was separated from the solid residue, two samples of about 50 ml were taken. One sealed for shipping and the second one was kept as a reference sample. The rest of the filtrate was discarded.
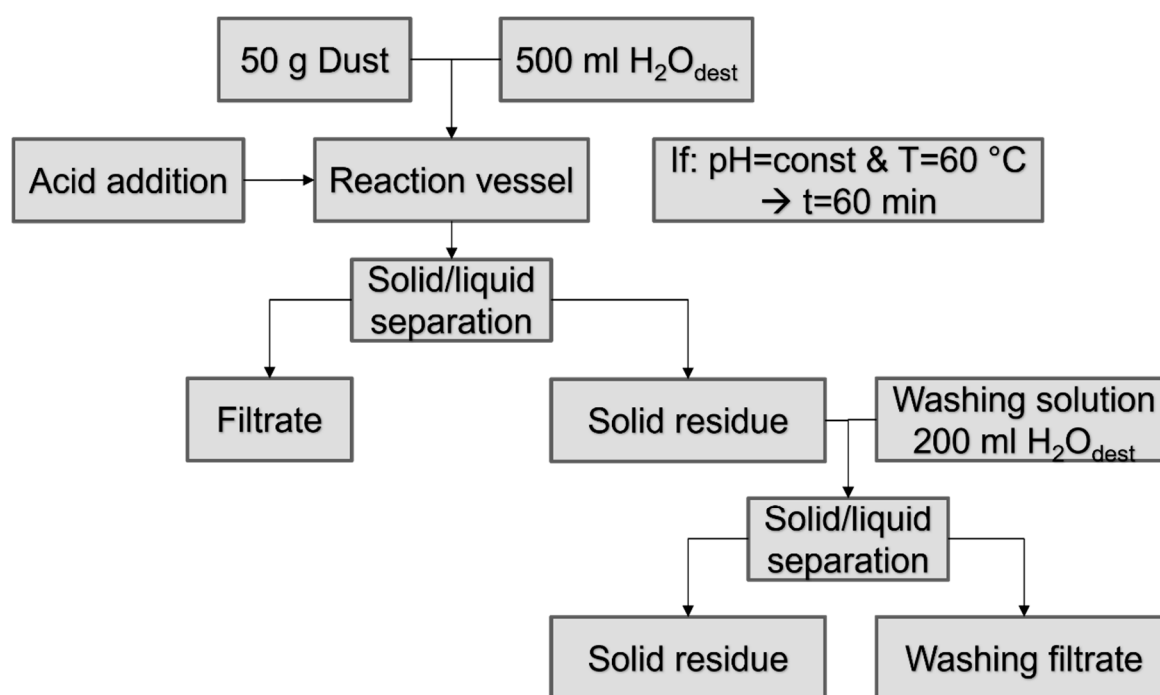
Figure 20: Flow sheet of the acid variation experiments

Furthermore, the still moist filter cake, which is still on the filter paper in the Büchner funnel, was treated with 200 ml of deionised water to wash any residual leaching liquid out. This was done to collect the residual leaching liquid hold by the filter cake to achieve a more accurate mass balance as well as more precise extraction rates. From the second filtrate another sample of about 50 ml was taken, sealed, and shipped for analysis. The now washed filter cake was removed carefully form the funnel and put on a heat resistant watch glass and put into a drying oven. The filter cake stayed in a furnace at 105 °C for at least 24 h or until mass constants was achieved. After this the sample was weight and a sample was prepared for shipping. The rest of the sample was kept for reference and future investigation.

6 Results

This chapter will present the data gained from the experiments. Extraction rates presented, were calculated on the base of the chemical analysis presented in Table 5. The company A.M.C.O. was again contracted to measure the contents of leached metals. For this the in Table 4 listed method for metals was used for all investigated samples.

6.1 Tentative campaign

Unfortunately, during the experiment the setup caused multiple problems, which made it impossible to exactly determine masses and volumes. Only the acid usage can be listed here. Furthermore, unlike for the acid campaign, no extraction rates could be determined, because of the unclear about filtrate volume.

Table 13: Measured experimental values after the tentative experiments

Experiment	Acid	V [ml]			m [g]
		acid usage	filtrate	evaporation	remaining dust
T1	HCl	45.5	-	-	-
T2	H_2SO_4	32.5	-	-	-

6.2 Acid variation campaign

The measured volumes and masses of the acid variation campaign are summarised in Table 14. In combination with the in Table 15 presented chemical analysis, extraction rates of each elements and for the used acids can be calculated by using the equations (1) to (3). The amount of metal recovered from the undried filter cake is calculated like the in (1) portrayed formula.

Table 14: Measured experimental values after the acid variation experiments

Experiment	Acid	V [ml]			m [g]
		acid usage	filtrate	evaporation	remaining dry dust
A1	HCl	45.5	495.0	50.5	33.915
A2	H_2SO_4	32.5	460.0	72.5	34.338
A3	HNO_3	23.5	447.5	76.0	42.870
A4	CH_3COOH	230.0	636.0	94.0	40.839
A5	$C_6H_8O_7$	264.0	687.5	76.5	34.678

In Table 15 the chemical analysis of the experiment A1 can be seen. The three different products are presented with each of their contents. The other chemical analysis of the product from the acid variation campaign can be seen from Table 19 to Table 22 in appendix.

Table 15: Chemical analysis of products from experiment A1

Element	Filtrate [mg/l]	Washing solution [mg/l]	Solid residue [wt-%]
Ca	22	1	3.3
Cr	844	5.8	7.3
Fe	21010	80	50.5
Mg	2.9	0.1	0.43
Mn	115	5.9	0.32
Mo	155	0.12	1.6
Ni	450	36	5.1
Zn	72	1.9	0.16
W	14.6	0.2	0.44

$$m_{Cr,\ filtrate} = c_{Cr,\ filtrate} \cdot V_{filtrate} \cdot 10^{-6} \qquad (1)$$

$$m_{Cr,\ dust} = m_{dust} \cdot \frac{\%\text{-}Cr_{dust}}{100} \qquad (2)$$

$$E_{Cr} = \frac{m_{Cr,\ filtrate} + m_{Cr,\ washing\ solution}}{m_{Cr,\ dust}} \cdot 100\% \qquad (3)$$

$m_{Cr,\ filtrate}$ .... mass of Cr in filtrate [g]

$m_{Cr,\ washing\ solution}$ ... mass of Cr in washing solution [g]

$c_{Cr,\ filtrate}$ .... concentration of Cr in filtrate [mg/l]

$V_{filtrate}$ .... volume of filtrate [ml]

$m_{Cr,\ dust}$ .... mass of Cr in dust [g]

m_{dust} .... mass of dust [g]

$\%\text{-}Cr_{dust}$ .... percentage of Cr in dust [wt-%]

E_{Cr}...................... extraction rate of Cr [%]

$$m_{Cr,\ filtrate} = 844\ \frac{mg}{l} \cdot 495\ ml \cdot 10^{-3}\ \frac{l}{ml} \cdot 10^{-3}\ \frac{g}{mg} = 0.448\ g$$

$$m_{Cr} = 50\ g \cdot \frac{6.6\ \%_{Cr}}{100\ \%} = 3.3\ g$$

$$E_{Cr} = \frac{0.448\ g + 0.001}{3.3\ g} \cdot 100\% = 12.66\ \%$$

The extraction rates for hydrochloric acid can be seen in Table 16. Noticeable are the high extraction rates of most acids for Fe, Zn and Mn which are around 30 %. Only the experiments conducted with HNO_3 show low leaching of all metals. Furthermore, HCl, H_2SO_4 and citric acid

managed to dissolve a medium amount of Cr, Ni, W. These concludes to a rate of about 10 % for these metals.

Table 16: Extraction rates of the different acids

Acid	Extraction rates [%]								
	Fe	Cr	Ni	Zn	W	Mo	Mn	Ca	Mg
HCl	37.5	12.7	9.9	35.6	8.0	11.8	27.8	1.7	1.0
H_2SO_4	34.7	9.4	9.4	34.0	62.4	42.5	25.6	1.6	1.25
HNO_3	14.3	3.7	5.0	3.0	2.5	3.2	18.3	0.2	1.0
CH_3COOH	21.13	5.6	5.43	42.0	29.1	33.7	25.4	1.1	1.3
$C_6H_8O_7$	34.25	8.5	7.0	37.2	75.6	52.0	34.9	1.0	1.3

Ca and Mg containing phases seem not to be dissolved well by any of the acid. Extraction rates for H_2SO_4 can be seen in. Noticeably high are the extraction rates with sulphuric and citric acid for the two refractory metals W and Mo.

7 Discussion

The following chapter discusses the results of both campaigns as well as the improvements made on the experimental setup.

7.1 Tentative campaign

Although the resulting data could not be used for a meaningful calculation of the extraction rates, nevertheless, the knowledge gained through these experiments were manifold. Therefore, based on these challenges, which came to attention, the optimizations are discussed here as well.

7.1.1 Extraction rate

As mentioned previously, the problems with the magnetic fraction when transferring the slurry caused the loss of material and leaching liquid. This made it impossible to calculate exact extraction rates.

7.1.2 Experimental setup

The setup used in this campaign was not optimal for the experimental investigation of the leachability of steel mill dust because of the reasons discussed in this paragraph. Non the less these crucial experiments gave important insights and led to the development of a new testing rig. One of the problems were caused through magnetic particles from the dust. These have gotten stuck on the magnetic steer bar which led to difficulties when pouring the solution into the filter for solid liquid separation. The particles, which got stuck on the steering bar could not be recovered from it without a significant loss of mass. This has led to the separate analysis of those two fractions. No technical useful magnetic separation was performed by this separation. But an idea formed that is to investigate the magnetic fraction, separated with a stronger magnetic grader. As a result of that, for the next experiment a glass stirrer attached to an agitator will be used, which will prevent the sticking of dust. Furthermore, no washing of the solid residue could be performed because of the significant loss during the cleaning of the stirrer. Therefore, a portion of the leaching liquid was lost as well and an exact mass balance from these experiments was not possible. Following this problem, a measuring of the volume of the leaching liquid could not have been conducted. Which further hindered the completion of a mass balance. Moreover, the usage of a dropping funnel was not an ideal solution for an accurately addition of the acid. This is because of the rather unsensitive valve and therefore hard to uncontrollable dropping of acid into the reaction vessel. To circumvent this, a disposable syringe attached with a flexible tube will be used in future experiments.

To summarize, the knowledge gained from the first campaign was an important insight on how such experiments need to be conducted. As can be seen when comparing Figure 17 to Figure 19 and Figure 23 the setup changed after every campaign to a more professional and optimized set up. The changes will be discussed in 7.2 and 8.1 in greater detail.

7.2 Acid campaign

The experiment conducted during this campaign showed promising results. Moreover, the setup allowed a better handling when transferring the slurry to the liquid solid separation. All changes made on the setup of the tentative campaign improved the outcome of these experiments. The results of this campaign will be discussed as follows.

7.2.1 Extraction rates

As can be seen in Table 16, extraction rates for each element have been varying from acid to acid quite in a large margin. Acids like HCl, H_2SO_4 and citric acid have performed quite well for the metals of interest. Vinegar acid did not leach Ni and Cr in the extend like the former mentioned, but performed quite well for Zn, W, Mo, and Mn simultaneously. Only HNO_3 did not leach any metal in a satisfactory fashion. The extraction rates for Cr and Ni over different acids are summarised in Figure 21 and Figure 22. In direct comparison of the two most promising candidates for further experiments, hydrochloric acid clearly shows advantages by leaching more Cr and Ni at lower temperatures and shorter times. HCl also shows promising properties when recovering spent acid after a potential leaching step. Furthermore, citric acid shows also extraction rates, when compared to HCl and H_2SO_4, even though it is a weaker organic acid. Moreover, the absence of Ca and Mg in any of the leching liquid is an indicator that these slag formers are not free in their lone oxide form in the dust. This is also noticeable in the XRD-analysis, where none of these phases could be identified. The are rather in a slag phase, which is most likely in glass form in the dust.

As mentioned in chapter 5.1, the identified phases should not be thermodynamically stable at pH-values below 0.3, which were being tested in the experiments. Therefore, it can be concluded that the kinetics of the leaching reactions must have been inhibited. To counter act this, the effect of longer leaching time and higher temperatures must be observed in future experiments.
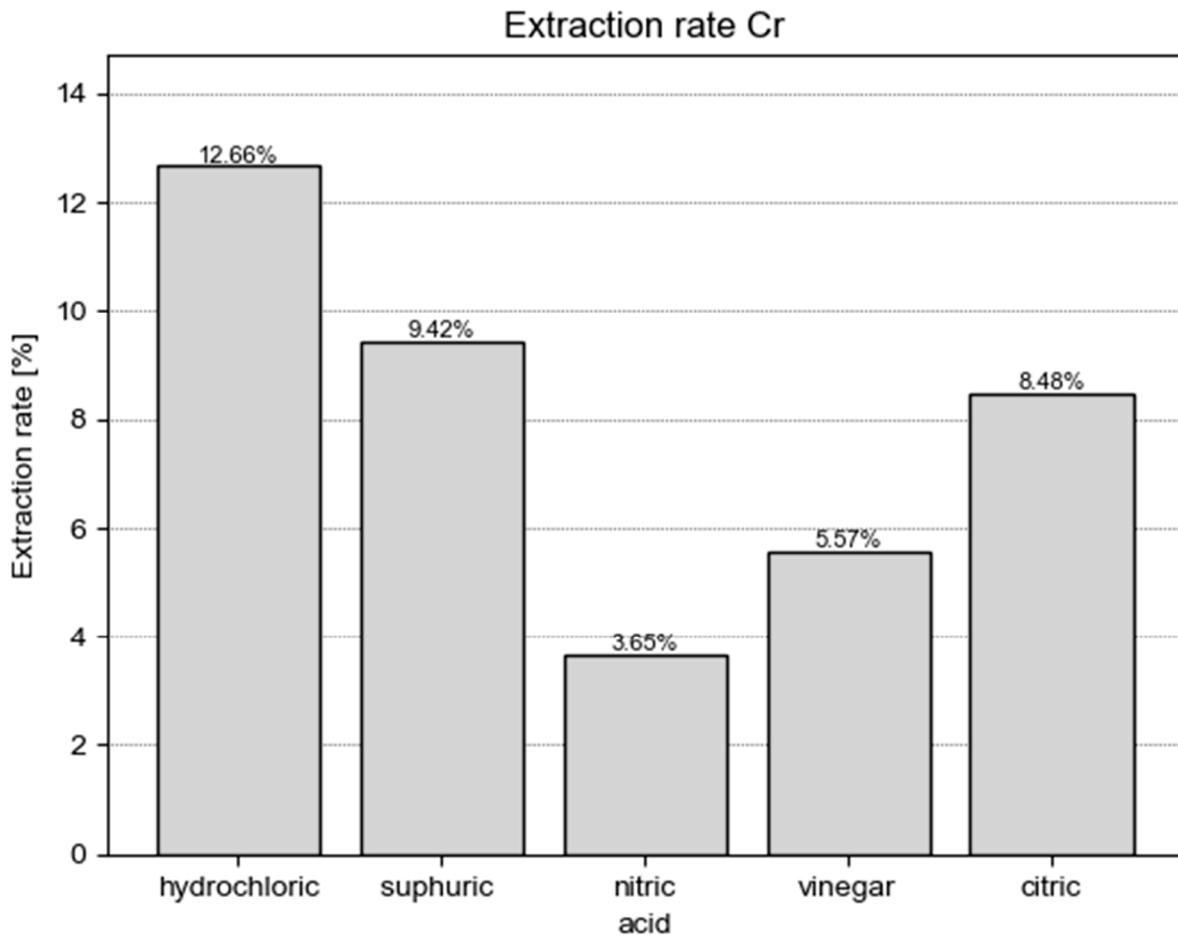
Extraction rate Cr

Figure 21: Comparison of extraction rates for Cr

The extraction rates of all acids for Zn as well as W must be interpreted with caution. The initial analysis of the EAFD shows only a limited amount of Zn and W in the dust. Therefore, it may be of interest to investigate dusts with a higher amount of these two metals.

Moreover, the lack of extraction of slag builders like Ca and Mg is positive in context of a possible separation from Cr and Ni. Even with citric and vinegar acid, the rates have been well below 2 %. This could be traced back to the lack of free and reactive amounts of CaO and MgO, which must be in a mixed phase with other slag forming phases like SiO_2 and Al_2O_3. Also, the lack of detection of neither of those phases in the XRD-analysis can be traced back to that.
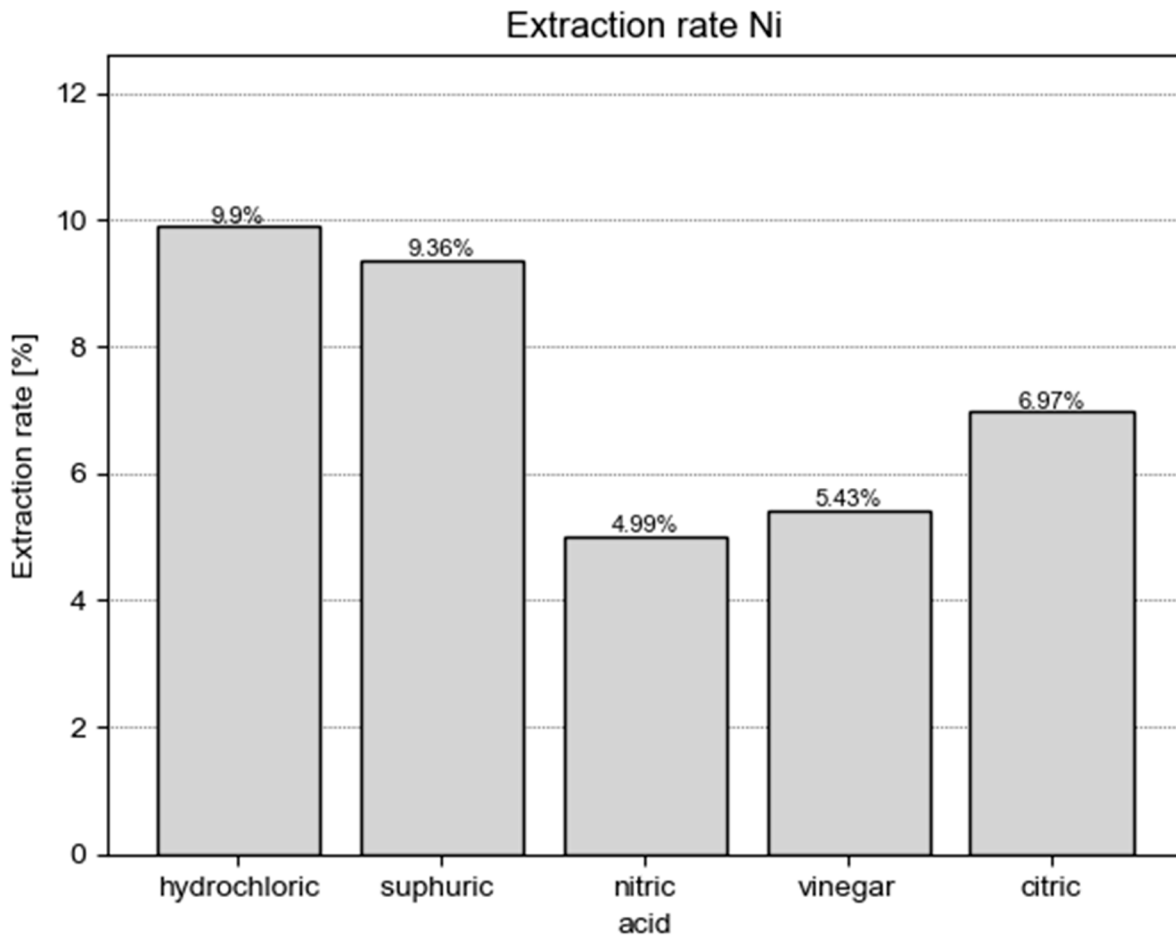
Figure 22: Comparison of extraction rates for Ni

7.2.2 Experimental setup

The experiments, which were performed with the setup depicted in Figure 19, produced acceptable data for the optimization of future experiments. Though the applied conditions of temperature, time and pH-value showed still optimization potential in context of extraction rates, they gave a valuable insight into the leaching operations. A future problem is the excess vaporisation of leaching liquid and therefore potential fluctuations in pH-value as well as evolution of potentially hazardous HCl containing gas. That these losses were not negligible even in this setup, can be seen in Table 14. Even though some improvements have been made regarding the experimental buildup compared to the tentative experiments of the first campaign, further development was necessary. The issues mentioned, are going to be addressed in the next development step which is described in chapter 8.1 and can be seen in the final setup for the future leaching operations in Figure 23.

8   Summary and prospect

In aspect of all previous mentioned literature as well as from the knowledge gained from the experiments, the following can be stated. The conducted experiments were satisfactory to the extent that first reliable data was acquired, as well as the setup was optimized to conduct the experiments properly for future leaching campaigns. Moreover, as can be seen in Figure 21 and Figure 22, hydrochloric acid is the most promising leaching agent, when compared to all the others used in this thesis. Nevertheless, a further campaign with citric acid, which showed reasonable extraction rates, at higher temperatures might be of interest.

8.1 Optimized experimental setup

An overhaul of the experimental setup was necessary, as mentioned before, to prevent previously observed challenges. As of the writing of this thesis, this has already been done and the first experiments have been conducted. The optimized setup can be observed in Figure 23. The previously used open-top beaker was substituted by a double walled reaction vessel, on which a lid with openings for other appliances can be placed. This closed system is especially suited for harsher conditions, like lower pH-value and higher temperature, to prevent vaporization and therefore loss of the leaching liquid. This vaporization prevention is supported by a reflux condenser, which can be attached to one of the openings. Connected with flexible plastic tubes to the side openings of the double walled reaction vessel is a circulating pump thermostat, which pumps heat-resistant liquid at reaction temperature into the hollow section of the reaction vessel. Because of all these improvements, the height of the whole reaction apparatus increased significantly. Thus, the previously used electrode was deemed too short, and a new pH-electrode had to be installed. The syringe performed so well in the last campaign that no improvements had to be made in that regard. Moreover, the agitator with the attached glass stirrer proved useful and does not to be changed for future campaigns.
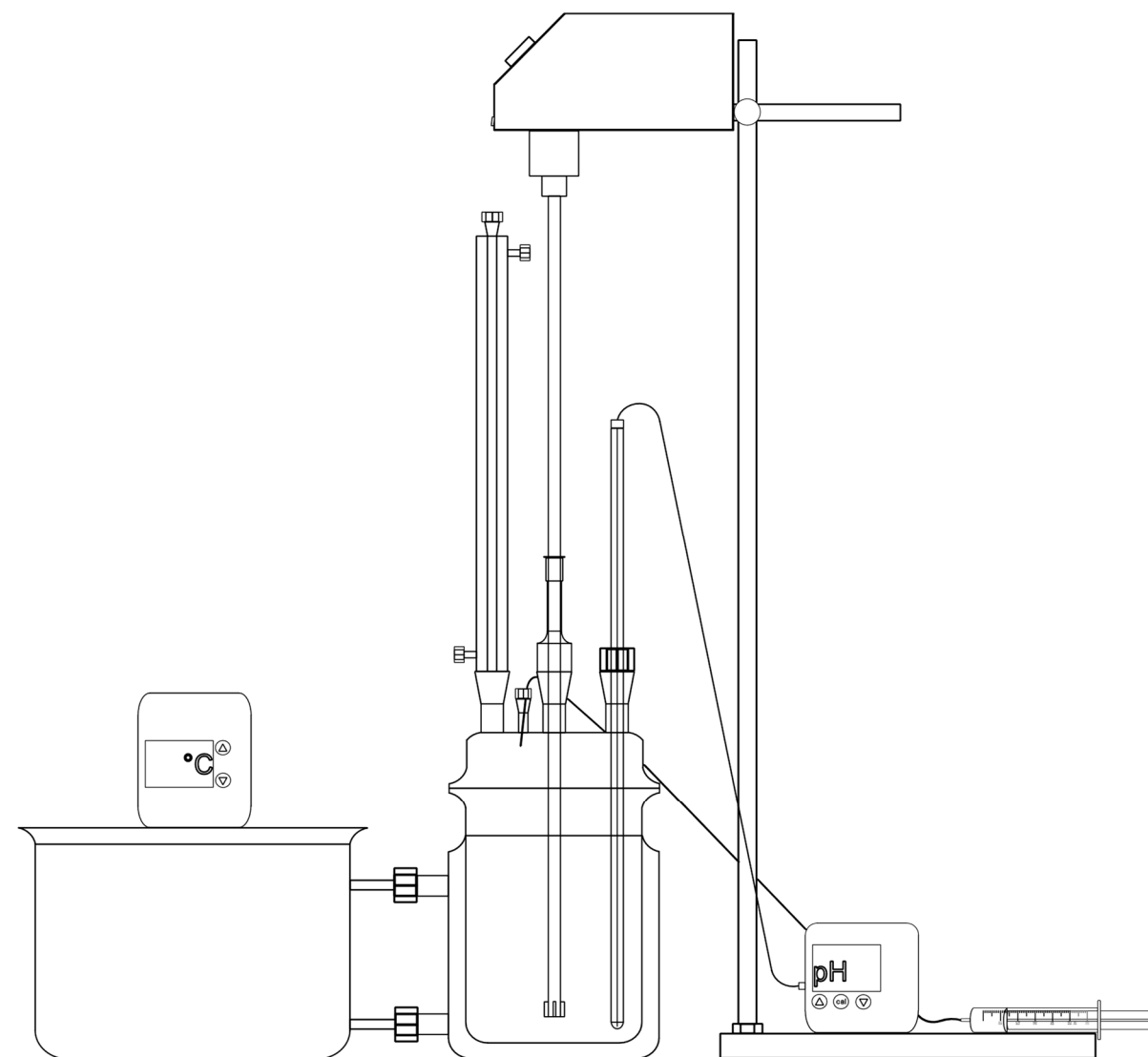
Figure 23: Improved experimental setup for higher temperatures and harsher conditions for complete mass balance

With a closed vessel plus a reflux condenser, the advantages of this setup are that vaporization and subsequent loss of the leaching liquid can be reduced to a minimum. Moreover, the utilization of a double-walled reaction vessel in conjunction with an external heating circulating pumping thermostat for more precise temperature control and faster heating are significant enhancements compared to the previously employed heating plate with thermal element.

As can be seen in Table 17, one of the main focuses of the planned campaigns will be an increase in temperature as well as leaching time. This will be of special interest because with increasing these two parameters separately as well as combined, their influence on the leaching reaction kinetics reaction can be observed.

8.2 Planned campaigns

The future campaigns will focus on HCl as leaching agent. To determine the optimal parameters for a potential industrial process, the focus of the currently planned experiments will lie on variation of parameters like temperature, time, solid to liquid ratio as well as the dust itself. The planned experiments can be observed in Table 17, which provides an overview of the parameters that will be investigated. As can be seen, this campaign will also investigate the leachability of a second EAF-dust, contrary to the previous campaign in which only investigated a single dust. Both dusts contain a reasonable concentration of Cr and EAFD_8 also contains a good amount of Zn, which is of additional interest. The chemical analysis of EAFD_8 can be seen in Table 18 in the appendix.

Table 17: Planned experiments for the evaluation of the leachability of stainless steel dust

Experiment	Dust	Dust mass [g]	Time [min]	Temp [°C]	S:L [g/ml]
1			60		
2			90	90	
3			120		
4			240		
5				50	1:10
6	EAFD_1	50	120	60	
7				70	
8				80	
9					1:5
10			120	90	1:15
11					1:20
12			60		
13			90	90	
14			120		
15			240		
16				50	1:10
17	EAFD_8	50	120	60	
18				70	
19				80	
20					1:5
21			120	90	1:15
22					1:20

Furthermore, in the course of the project a pretreatment of the dust with Na_2CO_3 and their influence of extraction rates is planned for 2024. For such a pretreatment the dust would be mixed with the Na_2CO_3 and heated to a certain temperature and later leached.

Moreover, to complete the to develop process, the leached metals will have to be reextracted from the filtrate. For regaining the leached metals, Fe-hydrolysis experiments for separating the Fe from the liquid, as well as precipitation experiment for the valuable metals are in planning.

9 List of literature

[1] world steel association: World steel in figures 2022. Internet: https://worldsteel.org/steel-topics/statistics/world-steel-in-figures-2022/#world-crude-steel-production-1950-to-2021 (Access: 2024-01-14, 3 pm).

[2] European Commission. Joint Research Centre.: Greenhouse gas intensities of the EU steel industry and its trading partners. Publications Office (2022).

[3] Remus R. et al.: Best available techniques (BAT) reference document for iron and steel production. In: EUR (Luxembourg. Online), Band: 25521. Publications Office, Luxembourg (2013).

[4] Statista research department: Global stainless steel melt shop production from 2005 to 2021. Internet: https://www.statista.com/statistics/223028/world-stainless-steel-production/ (Access: 2023-01-14, 4 pm).

[5] Gueaczennec A. G. et al.: Dust Formation by Bubble-burst Phenomenon at the Surface of a Liquid Steel Bath. ISIJ International, 44 (2004), 1328–1333.

[6] Guézennec A.-G. et al.: Dust formation in Electric Arc Furnace: Birth of the particles. Powder Technology, 157 (2005), 2–11.

[7] Delhaes C., A. Hauck and D. Neuschütz: Mechanisms of dust generation in a stainless steelmaking converter. Steel Research, 64 (1993), 22–27.

[8] Chung-Lee Li and Min-Shing Tsai: Mechanism of Spinel Ferrite Dust Formation in Electric Arc Furnace Steelmaking. ISIJ International, 33 (1993), 284–290.

[9] Stewart D. J. C. and A. R. Barron: Pyrometallurgical removal of zinc from basic oxygen steelmaking dust - A review of best available technology. Resources, Conservation and Recycling, 157 (2020), 104746.

[10] Xiaolong Lin et al.: Pyrometallurgical recycling of electric arc furnace dust. Journal of Cleaner Production, 149 (2017), 1079–1100.

[11] Hasegawa S., H. Kokubu and Y. Hara: Development of a Smelting Reduction Process for Recycling Steelmaking Dust. Ironmaking Technology and Tubular Products Technology, 38 (1998) online proceedings.

[12] Money K. L., R. H. Hanewald and R. R. Bleakney: Processing steel wastes pyrometallurgically at INMETCO. Proceedings of the TMS Fall Extraction and Processing Conference (2000), 397–408.

[13]   Zhang Huaiwei and Hong Xin: An overview for the utilization of wastes from stainless steel industries. Resources, Conservation and Recycling, 55 (2011), 745–754.

[14]   Denton G. et al.: EAF stainless steel dust processing. online proceedings (2005) online proceedings.

[15]   Schoukens A., D. G. Meyer and E. W. Giesseke: Environmental treatment of EAF-AOD dusts. International chromium development association (1996), 1–6.

[16]   Beskow K. et al.: The sustainability of valuable metals - recycling of residues from stainless steel production. Baosteel BCA (2010) online proceedings.

[17]   Joyner K. E.: FASTMET®/FASTMELT® : the final steps in waste recovery*. Rev. Met. Paris, 97 (2000), 461–469.

[18]   Pargeter J., R. Hanewald and D. Dombrowski: Operating experience at INMETCO and application of the process to the production of DRI. Conservation & Recycling, 8 (1985), 363–375.

[19]   voestalpine BÖHLER Edelstahl GmbH & Co KG: Overview production. Internet: https://www.bohler-edelstahl.com/de/produktion/ (Access: 2024-01-16, 11 am).

[20]   The European steel association: European Steel in Figures-2022. Internet: https://www.eurofer.eu/assets/publications/brochures-booklets-and-factsheets/european-steel-in-figures-2022/European-Steel-in-Figures-2022-v2.pdf (Access: 2024-01-14, 2 pm).

[21]   voestalpine BÖHLER Edelstahl GmbH & Co KG: Böhler in Zahlen. Internet: https://www.bohler-edelstahl.com/de/ (Access: 2024-01-20, 11 am).

[22]   Laforest G. and J. Duchesne: Characterization and leachability of electric arc furnace dust made from remelting of stainless steel. Journal of Hazardous Materials, 135 (2006), 156–164.

[23]   Majuste D. and M. B. Mansur: Characterization of the fine fraction of the argon oxygen decarburization with lance (AOD-L) sludge generated by the stainless steelmaking industry. Journal of Hazardous Materials, 153 (2008), 89–95.

[24]   Nolasco-Sobrinho P. J., D. C. R. Espinosa and J. A. S. Tenório: Characterisation of dusts and sludges generated during stainless steel production in Brazilian industries. Ironmaking & Steelmaking, 30 (2013), 11–17.

[25]   Stefanova A., J. Aromaa and O. Forsén: Alkaline leaching of zinc from argon oxygen decarbonization dust from stainless steel production. Physicochemical Problems of Mineral Processing, 49 (2013), 37–46.

[26] Sofilić T. et al.: Characterization of steel mill electric-arc furnace dust. Journal of Hazardous Materials, 109 (2004), 59–70.

[27] Schneeberger G. and J. Antrekowitsch: New developments in the recycling of zinc containing dusts from steel and foundry industry: Proceedings of European Metallurgical Conference EMC 2011, 1493–1506.

[28] Pawlek F. E.: Metallhüttenkunde. DE GRUYTER, Berlin (1983).

[29] Antrekowitsch J. et al.: Chapter 9 - Zinc and Residue Recycling. In: Worrell, E., Reuter, M. A. (Hg.): Handbook of Recycling. Boston: Elsevier, 113–124.

[30] Hanewald R. H. and D. E. Dombrowski: Recovery of metals from steel wastes and production of DRI by the INMETCO process. Iron and Steel Engineer, 62 (1985), 62–67.

[31] Hara Y. et al.: Smelting Reduction Process with a Coke Packed Bed for Steelmaking Dust Recycling. ISIJ International, 40 (2000), 231–237.

[32] Cyro T. et al.: Recovery of Cr, Ni and Fe from dust generated in stainless steelmaking. Mineral Processing and Extractive Metallurgy, 114 (2005), 201–206.

[33] Zhou Y. et al.: Green and efficient recovery of stainless steel dust by iron-bath direct reduction. Separation and Purification Technology, 308 (2023), 123005.

[34] BEFESA ScanDust AB: About Befesa ScanDust. Internet: https://scandust.se/en/ (Access: 2024-02-06, 10 am).

[35] Schoukens A. et al.: The Ennviroplas process for the recovery of Zinc, Chromium and Nickel from steel-plant dust. Electric Furnace conference proceedings (1996), 341–351.

[36] Schoukens A., F. Shaw and E. Ghemaly: The enviroplas process for the treatment of steel-plant dusts. Journal of the Southern African Institute of Mining and Metallurgy (1993), 1–7.

[37] Liu P. et al.: Efficient Utilization of Stainless Steel Dust and Chromium-Containing Slag by Carbothermal Direct Reduction: Synergistic Mechanism and Optimization Analysis. Journal of Sustainable Metallurgy, 8 (2022), 1877–1891.

[38] Drissen P. et al.: Recycling of EAF dust into the EAF especially from high alloy steelmaking. Revue de Métallurgie, 99 (2002), 341–347.

[39] Drissen P.: Recent Development in Slag Treatment and Dust Recycling. Steel Research International (2009) online proceedings.

[40] Oustadakis P. et al.: Hydrometallurgical process for zinc recovery from electric arc furnace dust (EAFD): Part I: Characterization and leaching by diluted sulphuric acid. Journal of Hazardous Materials, 179 (2010), 1–7.

[41] Aromaa J. et al.: New hydrometallurgical approaches for stainless steel dust treatment. Mineral Processing and Extractive Metallurgy, 125 (2016), 242–252.

[42] Majuste D. and M. B. Mansur: Leaching of the fine fraction of the argon oxygen decarburization with lance (AOD-L) sludge for the preferential removal of iron. Journal of Hazardous Materials, 162 (2009), 356–364.

[43] International Organization for Standardization. DIN EN ISO 11885:2009-09, Wasserbeschaffenheit- Bestimmung von ausgewählten Elementen durch induktiv gekoppelte Plasma-Atom-Emissionsspektrometrie (ICP-OES) (ISO_11885:2007); Deutsche Fassung EN_ISO_11885:2009, (2009).

[44] Deutsches Institut für Normung. DIN EN 14582:2016-12, Charakterisierung von Abfällen- Halogen- und Schwefelgehalt- Sauerstoffverbrennung in geschlossenen Systemen und Bestimmungsverfahren; Deutsche Fassung EN_14582:2016, (2016).

[45] Deutsches Institut für Normung. DIN 38405-1:1985-12, Deutsche Einheitsverfahren zur Wasser-, Abwasser- und Schlammuntersuchung; Anionen (Gruppe_D); Bestimmung der Chlorid-Ionen (D_1), (1985).

[46] Dr. H. Putz, Dr. K. Brandenburg: Match!3 - Phase analysis using Powder Diffraction, Version 3.16. Internet: https://www.crystalimpact.de/match (2023).

[47] Vaitkus A. et al.: A workflow for deriving chemical entities from crystallographic data and its application to the Crystallography Open Database. Journal of Cheminformatics, 15 (2023), 123.

[48] Metso Outotec: HSC Chemistry 10, Equilibrium Composition, Version: 10.3.7.1. Internet: https://www.hsc-chemistry.com/ (2024).

10 List of figures

11 List of tables

12 Appendix A

Table 18: Chemical analysis of EAFD_8

Elements [%]					
Al	0.45	Ca	8.7	Cl	0.13
Co	0.03	Cr	4.9	F	0.57
Fe	21.1	Mg	8.6	Mn	1.5
Mo	0.54	Ni	0.42	Si	1.9
V	0.02	W	0.15	Zn	23.2

Table 19: Chemical analysis of products from experiment A2

Element	Filtrate [mg/l]	Washing solution [mg/l]	Solid residue [wt-%]
Ca	22	1.3	3.7
Cr	676	19.8	7.5
Fe	20900	1200	53.5
Mg	3.8	0.14	0.5
Mn	114	8.9	0.34
Mo	600	15	1.1
Ni	458	30	5.8
Zn	74	48	0.18
W	122	0.48	0.24

Table 20: Chemical analysis of products from experiment A3

Element	Filtrate [mg/l]	Washing solution [mg/l]	Solid residue [wt-%]
Ca	2.5	0.44	3.5
Cr	269	1.3	8.4
Fe	8868	409	60
Mg	3.2	0.22	0.46
Mn	84	4.8	0.35
Mo	46	4.4	1.3
Ni	251	15	4.5
Zn	6.6	1.4	0.15
W	5.1	0.2	0.32

Table 21: Chemical analysis of products from experiment A4

Element	Filtrate [mg/l]	Washing solution [mg/l]	Solid residue [wt-%]
Ca	11	3.9	3.3
Cr	289	25	7.2
Fe	9201	292	55.7
Mg	2.8	0.43	0.4
Mn	82	7.3	0.33
Mo	344	2.2	1.2
Ni	192	45	5
Zn	66	3.9	0.14
W	41.2	1.3	0.34

Table 22: Chemical analysis of products from experiment A5

Element	Filtrate [mg/l]	Washing solution [mg/l]	Solid residue [wt-%]
Ca	8.6	1.4	3.2
Cr	407	35.3	5.8
Fe	13800	1170	53.3
Mg	2.56	0.3	0.4
Mn	104	7.27	0.32
Mo	492	40	1.0
Ni	228	18.8	5
Zn	54.1	2.35	0.17
W	99	12.3	0.24